M. J. MacLachlan et al.

DOI: 10.1002/anie.201407141

Liquid-Crystal Templates

Functional Materials from Cellulose-Derived Liquid-Crystal Templates

*Michael Giese, Lina K. Blusch, Mostofa K. Khan, and Mark J. MacLachlan**

Keywords:
cellulose · functional materials · liquid crystals · mesoporosity · photonic crystals

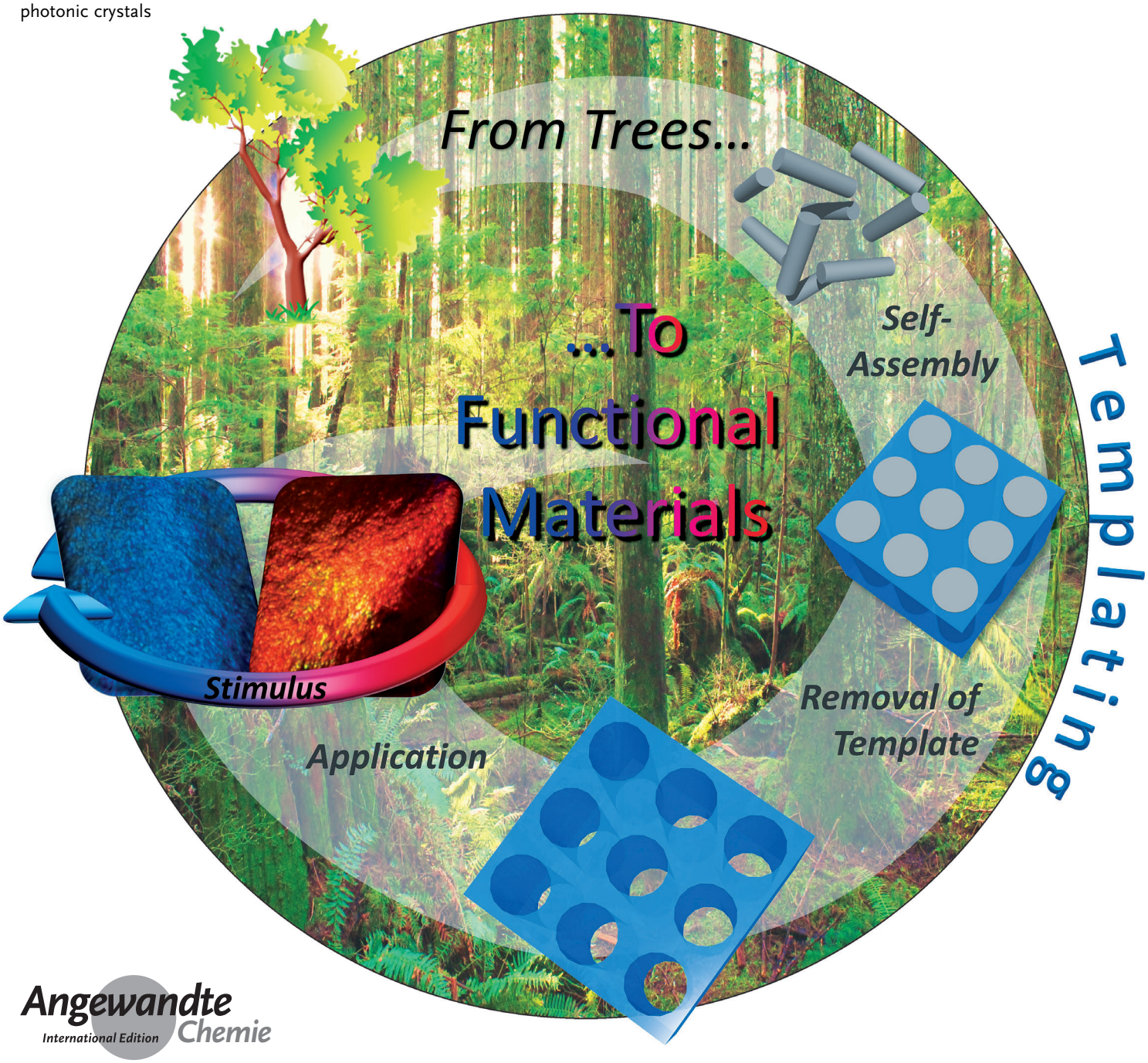

Cellulose nanocrystals (CNCs), known for more than 50 years, have attracted attention because of their unique properties such as high specific strength and modulus, high surface area, and fascinating optical properties. Just recently, however, their potential in supramolecular templating was identified by making use of their self-assembly behavior in aqueous dispersions in the presence of compatible precursors. The combination of the mesoporosity, photonic properties, and chiral nematic order of the materials, which are available as freestanding films, has led to a significant number of interesting and promising discoveries towards new functional materials. This Review summarizes the use of cellulose derivatives, especially CNCs, as novel templates and gives an overview of the recent developments toward new functional materials.

From the Contents

1. Introduction

Nanomaterials that have at least one dimension of 1 to 100 nm have gained tremendous interest because of their various applications in electronics,[1] optics,[2] magnetism,[3] energy storage,[4] and electrochemistry.[5] Reflected by the diversity of applications, the field of nanomaterials acts to unite physics, chemistry, materials science, engineering, and biology.[6] The rapid development in the field of nanostructured materials was closely related to the invention of new synthetic techniques. While most nanomaterials were initially prepared by top-down approaches (e.g. milling and lithography), the development of diverse bottom-up approaches allowed for precise control of the final morphology and composition of the nanomaterials.[7] Meticulous control of the dimensions, compositions, and defects plays a crucial role in creating high-performance functional materials.

An effective method for casting structural features on the nanometer length scale into materials is to employ templates with the desired structural architectures.[8] The self-assembly of templates allows for control of the dimensions, periodicity, and structure, thereby giving access to many new nanomaterials. Templates can vary from hard templates such as carbon[9] and silica[10] to soft templates[11] such as biomolecules[12] and polymers.[13] Soft templates need to show the ability to self-assemble into transferable superstructures. In this context, liquid crystals (LCs) are one of the most exciting templates, and they have been widely deployed.[14]

Common LCs are organic molecules with an anisotropic shape, such as mono- and disaccharides,[15] biphenylalkyl compounds,[16] surfactants,[17] and their polymeric analogues.[18] Diverse biopolymers such as DNA, silk, amyloids, chitin, collagen, and cellulose,[19] and even microorganisms can also exhibit liquid-crystalline behavior.[20] As a consequence of their shape anisotropy, LCs form characteristic mesophases—a state of matter that combines the long-range order of crystals with the mobility of an isotropic liquid. A rich polymorphism is observed, depending on the molecular shape and packing preferences of the mesogen (Figure 1). Diverse mesogens are known that vary in molecular shape (e.g. rod-like = calamitic and discotic) and their thermal behavior (thermotropic liquid crystals). Other substances only form liquid-crystalline phases in solvents (lyotropic liquid crystals, LLCs), where their phase behavior is dependent on both the concentration and temperature, as well as the pH value and the ionic strength of the solution.[21]

LLCs are widely used in templating, as their liquid-crystalline phase is compatible with a number of precursors.[22] LLCs can act as direct templates—a process that is known as "true LLC templating" or "soft templating"—or as structure-directing agents.[23] As structure-directing agents, LLCs provide a nanoreactor in which nanoparticles will be formed. The dimensions of nanoparticles are controlled by the liquid-crystalline phase; for example, a micellar cubic phase produces spherical nanoparticles and a lamellar phase gives platelike particles.[24] In contrast, soft templating leads to a solid, inorganic replica that is the negative image of the mesophase.

Liquid-crystalline phases have been observed in many biomolecules (e.g. lipids, cellulose, and DNA), but so far little is known about their function and contribution to structural templating within their natural environment.[25] It has been hypothesized that the chiral nematic phase of cellulose may support the building of helical plant walls[26] and that the liquid-crystalline behavior of DNA in sperm heads supports the separation of daughter chromosomes.[27] LCs derived from natural sources are exciting, sustainable alternatives to synthetic LCs as a result of their biocompatibility and high abundance. It was shown that, after isolation, collagen[28] and cellulose[29] are suitable natural LC templates for the synthesis of mesoporous silica.[28b,30] Chitin from crab shells and other sources has also been used to template mesoporous silica.[31,32]

Here we review the work that has been done to develop nanostructured functional materials derived from cellulose-based LC templates. In contrast to previous reviews on cellulose and cellulose nanocrystals, we focus on successful examples of soft templating using liquid-crystalline cellulose

[*] Dr. M. Giese, Dr. L. K. Blusch, Dr. M. K. Khan, Prof. M. J. MacLachlan
Department of Chemistry, University of British Columbia
2036 Main Mall, Vancouver, BC, V6T 1Z1 (Canada)
E-mail: mmaclach@chem.ubc.ca

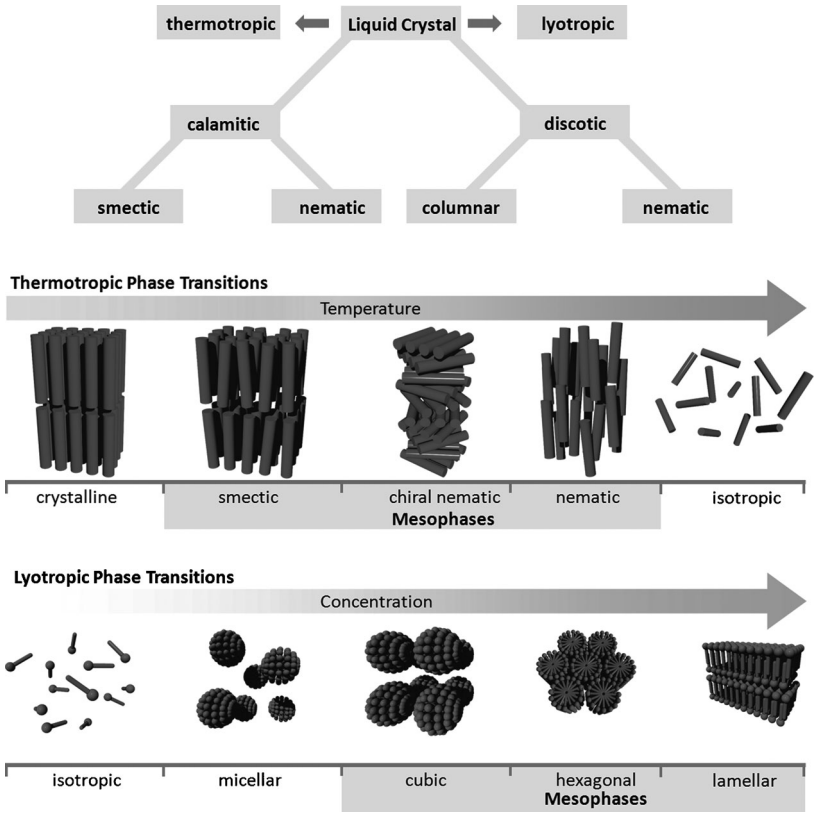

Figure 1. LCs can be categorized according to their shape (calamitic = rodlike or discotic) or their behavior (thermotropic or lyotropic). Thermotropic liquid crystals show temperature-dependent phase transitions in the pure form, whereas LLCs are formed in solution. The phase behavior of LLCs is dominated by the concentration of the mesogen, although it also depends on the temperature.

derivatives for the development of new functional materials. Initially we summarize the advantages and properties of cellulose-based LCs as templates then follow with an overview of synthetic procedures for generating nanostructured composite materials and the resulting mesoporous free-standing films. The final section of this Review highlights the intrinsic functionality arising from the imprinted nanostructure. Additional surface and pore functionalization as well as hard templating expand the range of applications, such as tuning of the structural coloration, selective reflection, imprinting of patterns, and sensing.

2. Cellulose-Based Liquid Crystals

Cellulose is the most abundant natural polymer produced in the biosphere, with an estimated annual production of more than 7.5×10^{10} tons.[33] The intrinsic biocompatibility and biodegradability of natural materials makes renewable, nontoxic, and inexpensive cellulose a highly relevant source for the development of sustainable functional materials. Cellulose is mostly isolated from plants, although it can also be extracted from several marine animals, fungi, and bacteria.[34] In nature, cellulose is found in fibers that consist of a bundle of microfibrils made by individual chains of β-(poly-1,4-D-glucose). Each microfibril consists of amorphous and crystalline

Michael Giese studied chemistry at the RWTH Aachen University, where he worked with Prof. M. Albrecht on anion–π interactions. After receiving his PhD, he joined the group of Prof. MacLachlan to work on nanostructured materials templated by cellulose nanocrystals. He is now working as Junior Professor for supramolecular functional materials at the University of Duisburg-Essen.

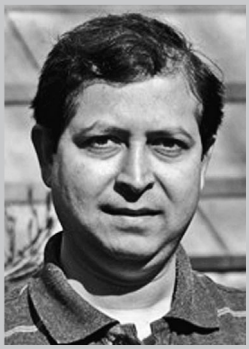

Mostofa K. Khan received his PhD from Carleton University, Canada, for his work on hydrogen-bond-mediated self-assembly of polyurethane model compounds under the supervision of Prof. P. R. Sundararajan. Since June 2011 he has been a postdoctoral fellow with Prof. MacLachlan, working on mesoporous photonic materials templated by cellulose nanocrystals.

Lina K. Blusch received her PhD from the University of Göttingen, Germany, on expanded porphyrin complexes and their redox chemistry in the group of Prof. F. Meyer. Since February 2013 she has been a Humboldt postdoctoral fellow with Mark MacLachlan. Her current research focuses on LC templating with CNCs.

Mark MacLachlan obtained his BSc in chemistry from UBC and his PhD in inorganic chemistry from the University of Toronto, where he worked with Profs. Ian Manners and Geoff Ozin. After 2 years as an NSERC PDF with Prof. Timothy Swager at MIT, he returned to UBC, where he is now a Professor of Chemistry. His work encompasses diverse areas, including macrocycles, tautomerization, coordination chemistry, MOFs, and solid-state materials.

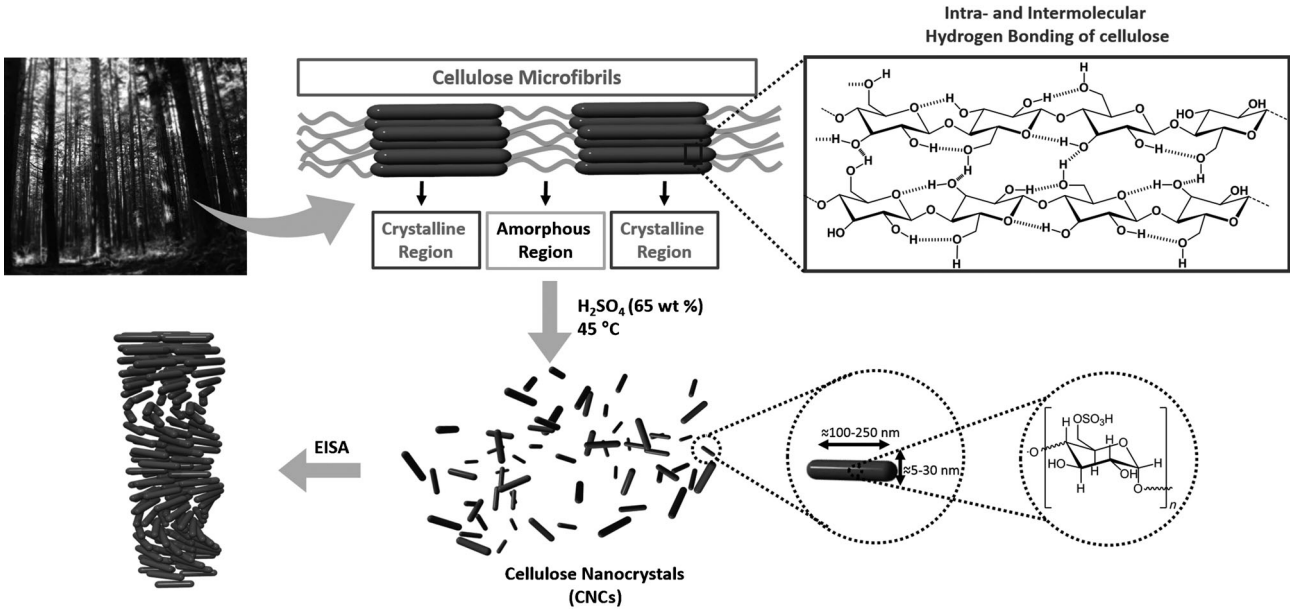

Scheme 1. The isolation of CNCs from trees follows two consecutive steps: After milling trees to soft wood pulp, the cellulose microfibrils are treated with H_2SO_4 at 45 °C to destroy the amorphous regions. The remaining CNC nanorods have dimensions of 5–30 nm in diameter and 100–250 nm in length, depending on the wood source. The sulfated surface introduces a charge and promotes the chiral nematic self-assembly.

parts, and a complex network of hydrogen bonds is formed.[35] In the 1950s, Rånby et al. developed a method to isolate cellulose nanocrystals (CNCs) from microfibrils by treatment with acid. Although the advantages and properties of CNCs have already been reviewed,[35,36] we briefly present the most important features of CNCs that are relevant to templating.

The acidic treatment of cellulose selectively hydrolyzes the amorphous parts of the biopolymer, thereby leaving nanocrystalline rods (Scheme 1).[37] Depending on the conditions for the acidic treatment and the source of cellulose, the size of these rods vary from 50 to 1160 nm in length and about 3 to 50 nm in diameter.[38] When sulfuric acid is used, some surface hydroxy groups are converted into sulfate esters. The simultaneous introduction of the negative surface charge stabilizes aqueous dispersions of CNCs through electrostatic repulsion.[39] In 1959, Marchessault et al. reported that CNC dispersions derived from sulfuric acid hydrolysis form lyotropic liquid-crystalline phases.[40] However, the specific self-organized phase of CNCs—a chiral nematic (cholesteric) phase—was not determined until 1992.[39] In the late 1990s, Gray and co-workers showed that the chiral nematic organization of the CNCs could be retained in solid films prepared by evaporation-induced self-assembly (EISA).[41] The term EISA is widely applied to this process, but it is important to note that the self-assembly actually occurs under thermodynamic (equilibrium) control in solution and the evaporation merely increases the concentration of the components in solution.

Today, CNCs are industrially prepared in large quantities from plants. In a typical procedure, bleached kraft softwood pulp is treated with 65 wt % sulfuric acid at 45 °C to give CNC rods about 5–30 nm in diameter and approximately 100–250 nm in length. After washing, the dispersion has a pH value of about 2.4 because of the acidic HSO_4 surface groups.[42,43] The resulting suspensions readily self-assemble at concentrations of 3–7 wt % into a chiral nematic phase that is retained in thin films after evaporation.

Films of CNCs bear chirality on three different scales: 1) on the molecular level because of the asymmetric carbon atoms of each D-glucose unit; 2) on the nanoscale because of the screw-shape morphology of the individual crystals; and 3) the left-handed chiral nematic long-range order of the lyotropic liquid-crystalline phase.[35]

Chiral nematic structures are frequently referred to as one-dimensional photonic crystals. Photonic crystals are materials with a periodically changing refractive index in one, two, or three dimensions; they can selectively diffract certain wavelengths of light.[44] In the case of a chiral nematic structure, the reflected wavelength depends on the pitch (P) of the chiral nematic structure and the refractive index (n_{avg}) of the substance.[45] The helical pitch corresponds to the repeating distance for a full 360° turn of the mesogens. When the half value of the pitch of the chiral nematic structure corresponds to wavelengths of visible light, the films appear iridescent (Figure 2). As a consequence of the chiral long-range order, light reflected from the chiral nematic LC is circularly polarized with a handedness that is determined by the helical orientation of the LC. Thus, a maximum of 50 % of the incident light will be reflected.

As a consequence of the surface sulfate esters on CNCs, the pitch of the chiral nematic LLC phase is highly sensitive to the ionic strength of the solution. By varying the ionic strength of the solution, one can control the pitch and, hence, the reflected color of the resulting films.[46] Higher ionic strengths reduce electrostatic repulsion between the CNCs, thereby leading to a smaller helical pitch. According to the equation in Figure 2, this finally leads to a blue-shift in the iridescence of the CNC films after EISA. However, color

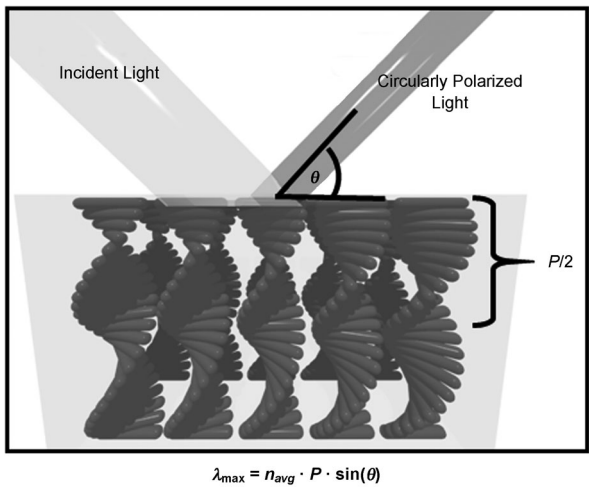

Figure 2. Selective reflection of circularly polarized light by a chiral nematic structure. The rods represent the average orientation of the director, which lies perpendicular to the films and rotates through the film.

tuning is only possible over a specific range of ionic strength, pH values, or precursor loading. Outside this range, the LLC phase is disturbed or completely lost by, for example, gelation.

The choice of the counterion (to the surface sulfate esters) also has a significant impact on the helical pitch and, thus, color tuning can be achieved by using the corresponding hydroxides for neutralization of CNCs.[47] It is found that increasing the van der Waals radii of the counterions, such as $H^+ < Na^+ < K^+ < Cs^+$, leads to an increased pitch and a red-shift of the maxima of the reflected wavelengths in the CNC films. The nature of the counterion also plays a crucial role with respect to the critical concentration for the formation of the chiral nematic phase, the stability of the films, the temperature dependence of the phase separation, and the re-dispersibility of the dried films.[46,48] In addition, the drying temperature,[49] external magnetic fields, and ultrasonication have a significant influence on the helical pitch.[50] Just recently, the substrate on which the CNC films are cast was identified as a further influential factor.[51] Ionic strength, the nature of the counterion, changes in temperature,[50] treatment of the CNC beforehand, and the casting substrate provide many handles to adjust the pitch of the CNC films, but once the films are dried, the color is virtually locked. Humidity can affect the color of CNC films, thus offering a way to sense moisture.[52]

The ability to form liquid-crystalline phases is not limited to pure cellulose but also applies to a number of cellulose derivatives, such as hydroxypropylcellulose (HPC), ethyl cellulose (EC), and chitin. Chitin is, after cellulose, the second most abundant polysaccharide and carries an acetamide function at its C2 atom. Its crystalline parts can be isolated after treatment of crustacean shells with acid. Aqueous suspensions of chitin show a critical concentration of about 10 wt% to form a chiral nematic phase.[53]

HPC and EC are synthetic cellulose derivatives prepared by alkaline treatment to yield alkali cellulose, followed by reaction with the respective alkyl chlorides.[54] However, much higher concentrations of the cellulosic derivatives are needed to form the chiral nematic phase than for CNCs (under 7 wt% for CNCs, 50–75 wt% for HPC, and around 40 wt% for EC).[55]

3. Preparation of Nanostructured Materials by Cellulose-Based Templates

The enormous interest in preparing nanostructured functional materials by a bottom-up approach has led to a variety of preparation techniques, such as layer-by-layer (LbL) deposition,[56] spin coating,[57] Langmuir–Blodgett deposition,[58] and molecular self-assembly.[59] However, simpler high-throughput methods are preferable to produce nanostructured materials on larger scales. In this respect, EISA is a promising approach to construct nanocomposites of cellulose. In general, this approach starts with a suspension of the LLC template and the addition of a compatible precursor to form a nanostructured composite material. Selective removal of the template from the composite gives porous materials (Scheme 2). This versatile, scalable method offers a route to

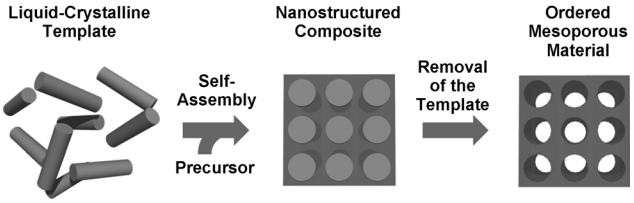

Scheme 2. Principle of soft LC templating: The LC solution is mixed with a precursor and allowed to self-assemble into a nanostructured composite. Subsequent selective removal of the LC template leads to a mesoporous negative hard copy of the LC mesophase.

diverse novel functional materials. Postsynthetic modification of the surface or the pores as well as hard templating enables further applications. An overview of commonly applied characterization techniques for analyzing the composites and mesoporous materials is given in Section 3.1. Various procedures for the cellulose-based templating approach are presented and their effect on the structural features of the inorganic and organic materials will be discussed (Section 3.2).

3.1. Characterization Techniques

Specific properties are introduced by the chiral nematic ordering, and several complementary characterization techniques are routinely employed to elucidate the nanostructure of templated materials. An optical microscope is indispensable to identify the chiral nematic order in the LLC and after drying in a film. Crystalline cellulose is optically biaxial with the largest refractive index oriented along the cellulose backbone and hence along the long axis of the nanocrystals.[35] In films, the nanocrystals are organized into layers where the rods are roughly aligned parallel to each other, but rotate through the stack; this organization resembles the Bouligand structure observed in the cuticles of many crustaceans and

insects.[26] The rotation of the nematic layers around the helical axis appears as periodic dark lines that resemble fingerprints when viewed under a polarized optical microscope (POM). When viewed between crossed polarizers, depending on the perfection of the pattern, significant areas of the chiral nematic films show birefringent square lattices with dark crosses that can be attributed to the parabolic focal conic defects trapped in the film structures.[60] The quasi-nematic layers with a left-handed helical twist can also be observed by scanning electron microscopy (SEM) at fracture cross-sections of the films, further corroborating their chiral nematic organization. As a result of the chiral nematic structure, the films exhibit photonic properties detectable by UV/Vis or circular dichroism (CD) spectroscopy. The appearance of reflection bands with exclusively positive ellipticity confirms left-handed chiral nematic structures. After removal of the template, the mesoporous materials have pore sizes in the range of 2 to 50 nm.[61] These porous structures have been investigated with respect to their gas-adsorption properties by applying Brunauer–Emmett–Teller (BET) theory and determining the Barrett–Joyner–Halenda (BJH) pore-size distribution.[62] Complementary to gas adsorption measurements, transmission electron microscopy (TEM) can also give information about the size and arrangement of pores in mesoporous materials.[63]

3.2. Synthetic Strategies

Several key issues have to be considered to guarantee a successful transfer of the structural features of the LLC phase into a new material. First, the precursors have to be compatible with the LLC phase and the solvent. Therefore, it is essential that the precursor and the LLC are of similar polarity and thus miscible. In addition, the concentration of the LLC as well as the ionic strength and pH value of the solution are crucial for compatibility. Ionic precursors or extreme pH values may cause gelation and disturb the LLC phase. Second, the kinetics of the condensation/polymerization reaction that form the new material have to be suitable to allow self-assembly of the template and formation of the LLC phase prior to complete solidification of the matrix around it. The precursor may undergo spontaneous polymerization or may be initiated by heating (curing) or irradiation with light. Third, any by-products of the polymerization around the template have to be highly volatile or compatible with the LLC phase of the cellulose-based template. If all of these parameters are considered, the LLC phase is formed above the critical concentration and a chemical reaction slowly "solidifies" the solvent to obtain a nanocomposite (Scheme 2).[14a] The template imprints the structural features of the LC phase as a negative copy into the resulting material and simultaneously acts as a placeholder to allow removal of the template to obtain porous materials with high surface areas.

Although composite films with chiral nematic order exhibit excellent properties themselves and can already act as functional materials,[64,65] the introduction of porosity further expands the range of potential applications for the materials. Selective removal of one component of a composite can be challenging, depending on their connectivity and compatibility. For a given composite material, it is necessary to find conditions that allow the selective removal of one component without adversely affecting the other. Furthermore, it is critical to find conditions that prevent the complete collapse of the network after removal of the template.

Calcination under air is the most common and simplest approach to remove organic templates from organic–inorganic composites. Cellulose-based templates usually decompose at temperatures above 250 °C in air. However, milder removal conditions, such as the acid- and base-catalyzed hydrolysis of the cellulose, are required to selectively remove the cellulose from more sensitive networks.

The removal of the template has a significant influence on the structure and photonic properties of the resulting mesoporous samples. Removing the cellulose template (refractive index, $n = 1.51$)[66] results in the creation of pores filled with air (refractive index, $n = 1.00$), thus causing a net reduction in the average refractive index of the mesoporous material and thereby a blue-shift in its reflected color. Calcination may also induce a contraction of the films that affects the pore-size distribution and causes a blue-shift.

3.2.1. Inorganic Materials

The most common reaction among LLC templating approaches is the synthesis of mesoporous silica, first reported by Kresge et al. in 1992.[67] This method has since been extended to the synthesis of porous materials with various structures and compositions.[68] Cellulose derivatives such as EC,[54b] HPC,[54a] and CNCs are employed as templates to form nanostructured materials. However, the need for much higher concentrations of EC and HPC to form the chiral nematic phase complicates the use of these cellulosic derivatives in soft templating—the increased viscosity arising from the high concentrations requires special handling and slows self-assembly.

Nevertheless, in 2003 Thomas and Antonietti reported the first nanocasting approach with silica by employing HPC as a soft template.[69] Silica composites were obtained by mixing aqueous HPC with tetramethyl orthosilicate (TMOS) in the presence of hydrochloric acid. The mixture was stored for several days to weeks in a sealed tube to allow the formation of the LLC phase (Figure 3a). After observation of the visible iridescence of the mesophase, the solvent was slowly evaporated under vacuum to obtain chiral nematic composites. Although the chiral nematic order of the HPC was clearly maintained in the composite, the retention of the chiral nematic long-range order was not evident in the calcined silica. The free-standing silica films, investigated by TEM and wide-angle X-ray scattering (WAXS), show mesoporosity (BET surface areas of 568–1135 $m^2 g^{-1}$) introduced by the removal of the cellulose-based template.

In 2010, Wang et al. synthesized ethylcyanoethylcellulose/poly(3-(methacryloyloxy)propyltrimethoxysilane) (E-CE)C/P(MPTOS) composites.[70] The composites were obtained by mixing 3-(methacryloyloxy)propyltrimethoxysilane (MPTOS), divinylbenzene (DVB, cross-linker), and an ini-

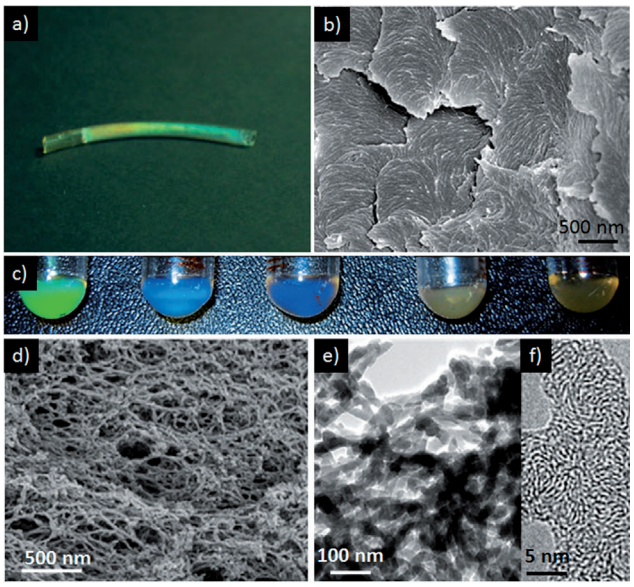

Figure 3. Photograph of the HPC/silica mixture showing the formation of the liquid-crystalline phase as observed by Thomas and Antonietti; b) SEM characterization of the (E-CE)C/P(MPTOS) composites; c) photographs of the chiral nematic phases of (E-CE)C/P(MPTOS) in acetic acid with various compositions as observed by Wang et al.; d) SEM and e,f) TEM micrographs of the silica samples from Wang et al. after calcination. Reproduced and adapted by permission of John Wiley and Sons and Springer.[69,70]

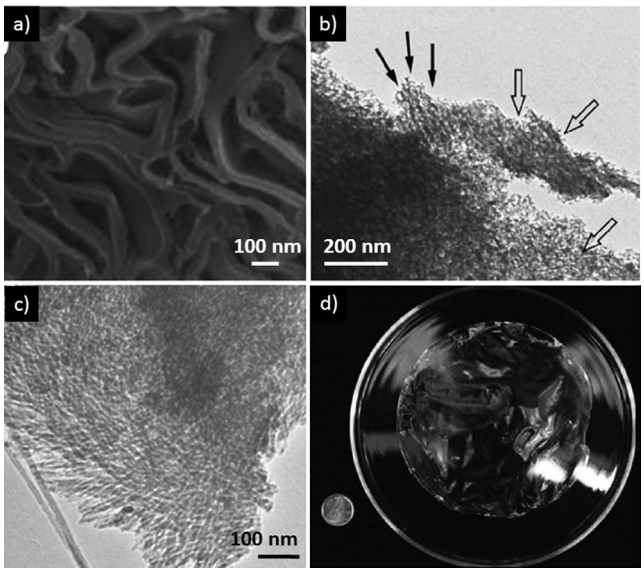

Figure 4. a) SEM images of porous titanium nitride as observed by Qi et al.; b) TEM micrographs of the mesoporous silica samples reported by Dujardin et al. (arrows show the in-plane (solid) and out-of-plane (hollow) projections of the porous structure); c) TEM image and d) a photograph of the chiral nematic mesoporous silica films by MacLachlan and co-workers (a dime is shown for scale). Reproduced and adapted with permission from John Wiley and Sons, Nature Publishing Group, and The Royal Chemical Society.[30,42,71,74]

tiator with ethylcyanoethylcellulose (E-CE)C in acetic acid. The clear mixture was allowed to sit for two weeks at room temperature in the dark to form the chiral nematic phase (Figure 3c). The mixture was then sandwiched between two glass slides and irradiated with UV light to initiate the polymerization. After a final drying at 40 °C under vacuum, residual acetic acid was removed and transparent films with a chiral superstructure were obtained, as proven by SEM (Figure 3b). After calcination of (E-CE)C/silica composites at 550 °C in air, porous silica with BET surface areas of 330–837 $m^2 g^{-1}$ and BJH pore-size distributions of 4.8 to 9.5 nm was obtained. SEM (Figure 3d) and TEM analysis (Figure 3e,f) of the silica materials revealed that the morphology of the silica materials is dependent on the silica precursor content in the composite.

In the same year, MacLachlan and co-workers used the self-assembly of cellulose in liquid NH_3/NH_4SCN solutions to form cellulose/metal nitride complexes.[71] A LC phase (ca. 8% w/v) or a gel (30% w/v) was obtained, depending on the cellulose concentration. After generating the LC or gel phase, a metal-containing precursor ($Ti(NEt_2)_4$ or VCl_4) was added to yield titanium and vanadium nitride/cellulose composites upon removal of the ammonia. Following calcination under flowing NH_3, nanoporous titanium or vanadium nitride was obtained as flaky black powders with BET surface areas of 80–600 $m^2 g^{-1}$. SEM (Figure 4a) in conjunction with gas adsorption analysis confirmed that the materials exhibit high porosity ranging from micro- to meso- to macropores depending on the cellulose-to-metal precursor ratio. No long-range chiral nematic order was observed in these liquid-crystal-templated materials, but they showed an unusual morphology that likely arises from the liquid-crystalline order of cellulose in liquid ammonia.

Nanocrystalline chitin (NCh) is also known to form a LLC phase, and researchers have recently investigated the ability of this material to form chiral nematic composites. Belamie and co-workers and Nguyen et al. formed nanocomposite materials of NCh and silica or organosilica by EISA.[31,32,72] No evidence for chiral nematic order was found in the composite materials, although evidence for a layered nematic structure in the composites was provided by electron microscopy investigations.

As already mentioned, the use of cellulose derivatives such as EC and HPC has significant drawbacks with respect to scaling up because of their high viscosities and slow organization. In contrast, CNCs with their nanoscale dimensions, anisotropic shape, high surface area, and fast formation of the LLC phase at low concentrations in aqueous suspensions have significant advantages for use in templating.[54c] The undisturbed co-condensation of various inorganic and organic precursors in the presence of CNCs makes the EISA approach highly promising for the development of new routes to functional materials with chiral nematic structures.

The first example to employ CNCs in templating was reported in 2003 by Mann and co-workers.[30] The addition of a prehydrolyzed solution of TMOS to an aqueous suspension of CNCs yielded a CNC/silica composite upon EISA. The material appeared birefringent before and after calcination. Although the calcined silica appears mesoporous, as indicated by TEM (Figure 4b), the imprint of the chiral nematic phase could not be proven unequivocally. In 2007, Shin and Exarhos

prepared porous titania films by CNC templating.[73] In the first step, a titanium(IV) bis(ammonium lactate) dihydroxide (Tyzor-LA) precursor was mixed with CNC suspensions to obtain a white composite by precipitation. Centrifugation gave a free-standing film that was dried under ambient conditions. However, the conditions employed did not maintain the characteristic chiral nematic structure of the CNCs.

The examples reported so far employed the self-assembly of cellulose-based templates to obtain nanostructured composite materials. However, the chiral nematic order of the template was not maintained in the matrix after removal of the template.

In 2010 Shopsowitz et al. discovered that alkoxysilane precursors such as TMOS or tetraethyl orthosilicate (TEOS) are compatible with the self-assembly of CNCs in aqueous suspensions, leading to homogeneous composites with vibrant iridescent colors.[42] The reflected color of the films was tuned from the UV to the near-IR region of the electromagnetic spectrum by the addition of salt or by varying the silica/CNC ratio.[75] Intense signals with positive ellipticity were measured by CD spectroscopy at the same wavelength as measured by UV/Vis spectroscopy, thus indicating that the reflection is circularly polarized exclusively in a left-handed manner and confirming that the chiral nematic structure of the CNCs was successfully transferred to the composite. The EISA was found to occur within a narrow pH range of the suspension (about pH 2.5 to 4). Achiral and optically opaque composites were obtained outside of that range. Since the refractive indices of CNCs and silica are similar, the shift in the reflected wavelength is predominately assigned to a change in the helical pitch. Removal of the cellulose by calcination yielded mesoporous silica films, with their iridescence attributed to their chiral nematic structure. TEM micrographs (Figure 4c) as well as nitrogen adsorption measurements on the calcined silica films prove the mesoporosity, with high surface areas ranging from 300 to 800 $m^2 g^{-1}$ and pore volumes of 0.25 to 0.60 $cm^3 g^{-1}$, depending on the compositions. The BJH pore size distributions give maximum pore diameters ranging from 3.5 to 4.0 nm, which suggests the successful replication of individual CNCs instead of their bundles in the pore structures. This pore size is smaller than the diameters of the individual CNCs used as a template and shows that the silica pore walls contract during calcination, thereby resulting in a blue-shifted reflected color compared to their corresponding composite films. The strong iridescence and birefringence of the calcined films, clearly observed under a polarization microscope, stem from the anisotropy of the mesoscopic ordering of the pores induced by self-assembly of the CNC. These were the first examples of chiral nematic mesoporous silica films.

Severe cracking arising from capillary pressure gradients during the last stages of drying is often observed, which poses a significant limitation for applications. Kelly et al. found that adding simple polyols (e.g. glucose) to the CNC dispersion before EISA alters the sol–gel curing kinetics[76] and reduces cracking of the composite films, thereby enabling large, crack-free homogeneous films to be created.[74] Calcination of the composites affords crack-free silica films with diameters of about 15 cm (Figure 4d). The data indicate that this modification does not significantly affect the optical properties or mesoporosity of the synthesized silica films. High-resolution SEM confirms the efficient replication of the chiral nematic ordering of the CNCs into these sol–gel derived materials.

The silica-based approach has been extended to other sol–gel precursors of the type $(RO)_3Si\text{-}R'\text{-}Si(OR)_3$ ($R' =$ aliphatic, aryl) to produce periodic mesoporous organosilicas.[77] Incorporation of organic spacers allows for improvement of the mechanical properties of the glassy materials and for incorporation of additional functionality. An alternative procedure for the removal of CNCs to generate organosilica materials was developed to prevent the thermal degradation of the organic linkers. Treatment with 6 M sulfuric acid at 100 °C for 18 h selectively removes the CNCs without affecting the chiral nematic structure of the organosilica matrix. Subsequent rinsing of the matrix with H_2O_2/H_2SO_4 solution washes out any remaining by-products from the decomposition of the cellulose to yield transparent and completely colorless films that become iridescent after drying (Figure 5a). Although the

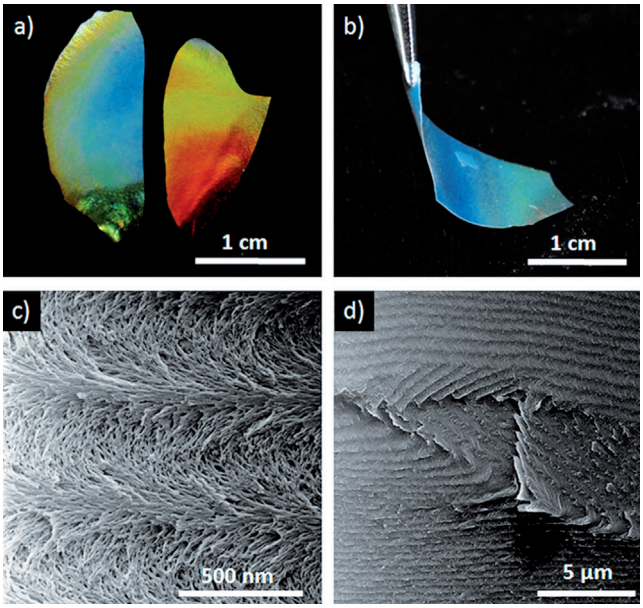

Figure 5. a) Photographs of chiral nematic ethylene-bridged organosilica films showing their iridescence and b) flexibility; c, d) their twisted layer nanostructure in the HIM micrographs. Reproduced and adapted with permission from the American Chemical Society and The Royal Society of Chemistry.[77,78,81]

selective removal of CNCs from alkyl-bridged organosilica composites could be accomplished with H_2SO_4, this procedure results in yellow organosilica films with phenylene-bridged silica.[78] The coloration can be attributed to sulfonation of the aryl groups. As a result, an alternative CNC hydrolysis procedure was developed using HCl followed by a silver-activated H_2O_2 rinse. Complete removal of the CNCs and retention of the organosilica in the pore walls were confirmed using solid-state ^{13}C and ^{29}Si cross-polarization magic-angle-spinning (CP/MAS) NMR spectroscopy. In comparison with brittle silica films synthesized from silica precursors (TMOS), organosilica films prepared with bridg-

ing organic groups have significantly improved mechanical properties in terms of their flexibility and tensile strength (Figure 5b). Nitrogen adsorption analysis reveals that mesoporous organosilica films also have high surface areas. The observed pore volumes (0.6–1.0 $cm^3 g^{-1}$) and pore diameters (8–9 nm) match the average diameters of CNCs measured by electron microscopy. Thus, the template-removal method (acid extraction versus calcination) indirectly offers a method to control the pore diameter and pore volume of the resulting materials. The mesopores in the organosilica materials could be visualized by helium ion microscopy (HIM), a technique that allows these insulating materials to be imaged directly without a conductive coating, and revealed fascinating details of their morphology (Figure 5c,d).[78] The long-range order in the materials was evident and, at high magnification, the individual mesopores could be visualized. The average pore diameter measured by HIM was found to be (8.4 ± 2.1) nm, which is in good agreement with the pore diameters measured by nitrogen adsorption analysis.

It is possible to incorporate additional functionality into the chiral nematic materials by surface functionalization. This method can introduce new components or improve the compatibility between the surface and guests. Hydrophilic pores of chiral nematic mesoporous ethyl-bridged organosilica films were made hydrophobic by functionalizing the organosilica surface with 1-(triethoxysilyl)octane.[79] Detailed elemental analysis (EA) and thermogravimetric analysis (TGA) studies showed the degree of functionalization of octyl groups to ethylene bridges to be approximately 1:10. This derivatization was used to improve the compatibility between potential hydrophobic guest molecules and the organosilica surface. Not much else has been done to directly modify the surface of the cellulose-templated materials, and this is an area of interest for further exploration.

Shopsowitz et al. developed an inexpensive and straightforward method to synthesize mesoporous carbons with high specific surface area, large pore volume, and chiral nematic order.[80] In their procedure, CNC/silica composite films are first synthesized by the same procedure as used to prepare iridescent, mesoporous silica films.[42] Pyrolysis of the CNC/silica composite films under nitrogen at 900 °C resulted in carbon/silica composites. TGA shows that the conversion of CNC into carbon yields 30 wt % mesoporous carbon. Free-standing mesoporous carbon films were obtained by selective etching of silica with aqueous base. The resulting material appeared as glossy black films that were composed of 90 % carbon and 1 % hydrogen, as measured by EA. The remaining 9 % consisted mostly of oxygen with trace amounts of sodium and silicon, as confirmed by energy-dispersive X-ray (EDX) analysis. Powder X-ray diffraction (PXRD) and Raman spectroscopy confirmed that pyrolysis of CNC films under inert conditions results in amorphous carbon. The porosity of the carbon films varies with the silica loading. Carbon films prepared directly from CNCs show mostly microporosity, whereas samples prepared with 65 wt % CNCs and silica were completely mesoporous. The surface area and pore volume of the mesoporous samples were 570–1460 $m^2 g^{-1}$ and 0.3–1.2 $cm^3 g^{-1}$, respectively, depending on the compositions. SEM analysis of these samples revealed a twisting helical morphology similar to their corresponding silica samples, thus indicating chiral nematic ordering.

3.2.2. Organic Materials

In addition to the inorganic composites presented in the previous section, a number of cellulose polymer composites have also been reported. In many studies, CNCs were employed to reinforce the mechanical properties of organic polymers because of their high Young's modulus.[82] After the first report by Favier et al. on a poly(styrene-*co*-butylacrylate)-based CNC nanocomposite in 1995,[83] the scope of reinforced polymers by the addition of CNCs expanded rapidly.[84] However, here we focus on the use of cellulose-based LLCs for imprinting the chiral nematic structure of the mesophase into a polymeric network. Polymerization of the monomers can occur during or after EISA, induced by acid, base, or irradiation with UV light.[54a,85]

HPC-based organic templating approaches yielded composite materials of poly(amic acid) and HPC, where the presence of chiral nematic order was proven by POM.[86] The chiral nematic structure was destroyed after removal of the HPC. Fernandes et al. prepared HPC films reinforced with CNCs that mimic the iridescent petals of the Queen of the Night tulip.[87] Liao et al. reported on polyacrylic acid/HPC[54a] composite nanogels, in which the HPC prevents bulk polymerization. No attempt was undertaken to remove the HPC from the composite. A similar strategy was followed with EC: EC was employed in the fabrication of polyaniline (PANI) nanofibers, where the length of the PANI chains was directed by the EC. The EC was successfully removed by solvent extraction after the polymerization of aniline was complete.[88]

In 2012, Tatsumi et al. reported a poly(2-hydroxyethyl methacrylate) (PHEMA) CNC composite.[89] Phase separation resulted in three clear composite films being obtained, one from the isotropic (PHEMA-CNC_{iso}), a second from the anisotropic (PHEMA-CNC_{aniso}), and a third one from the mixed phase (PHEMA-CNC_{mix}). Whereas the anisotropic sample shows a homogeneous fingerprint texture under POM (Figure 6a), which indicates a chiral nematic structure, the isotropic film shows only small regions with a fingerprint pattern. SEM on the anisotropic sample shows the helical twisting layered structure that is characteristic of the chiral nematic order in films (Figure 6b). Unfortunately, the helical pitch of the hydrogels is too large to show photonic properties, but all three samples showed a significant improvement in their thermal and mechanical properties relative to PHEMA.

In 2013, Kelly et al. reported novel photonic nanocomposite hydrogels with chiral nematic order that were prepared by the self-assembly of an aqueous CNC dispersion with various hydrogel monomers,[65] including acrylamide (AAm), *N*-isopropylacrylamide (NIPAm), acrylic acid (AAc), 2-hydroxyethyl methacrylate (HEMa), polyethylene glycol dimethacrylate (DiPEGMa), and polyethylene glycol methacrylate (PEGMa). Each non-ionic monomer was combined with a cross-linker (*N*,*N*′-methylenebisacrylamide (bis)) and a photoinitiator in an aqueous suspension of the CNCs. After EISA, the structures were locked in place by UV-initiated polymerization. Nanocomposite hydrogels with various

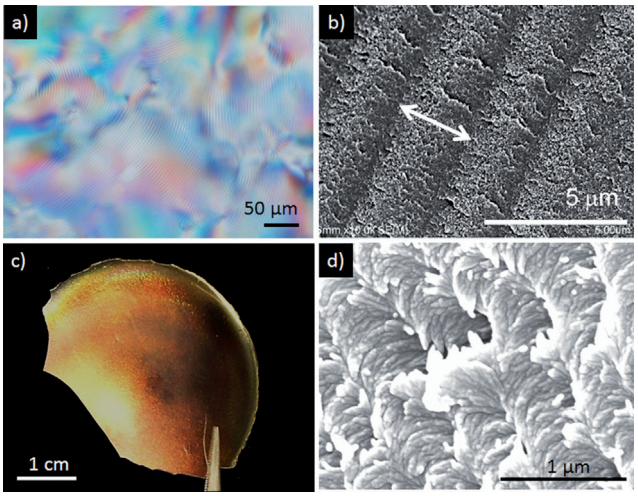

Figure 6. a) POM image of the lyotropic liquid-crystalline phase of an aqueous CNC suspension in the presence of HEMA and b) a SEM micrograph of the resulting polymer/CNC composite as reported by Tatsumi et al.; c) photograph and d) SEM image of the iridescent chiral nematic polymer/CNC composites as shown by Cheung et al. Reproduced and adapted with permission from the American Chemical Society.[47,89]

reflected colors were produced by increasing the ionic strength of the dispersion.

Until recently, a chiral nematic order of CNCs was only observed in water or aqueous solutions. This presents a substantial limitation to the precursors that can be employed—many precursors are unstable in water, insoluble in water, or condense too quickly to allow for the organization of the CNCs. Therefore, a straightforward method to disperse CNCs in organic media is desirable and will open the route to new composite materials. Attempts have been made to achieve this goal by using surface modification of CNCs by, for example, silylation,[90] grafting,[91] or simply coating with an anionic surfactant.[92] In some cases, the modified CNCs were shown to form chiral nematic phases in organic media, but these structural features were not retained in dried films.

Cheung et al. reported that neutralization of the acidic form of CNCs (CNC-H) with various strong bases, such as alkali metal and quaternary ammonium hydroxides, followed by freeze-drying produces the neutralized form of CNCs (CNC-X, X = Li^+, Na^+, K^+, NH_4^+, NMe_4^+, NBu_4^+).[47] CNC-Xs are readily dispersible in polar aprotic organic solvents such as dimethylsulfoxide (DMSO), formamide, *N*-methylformamide (NMF), and dimethylformamide (DMF). Fourier transform infrared (FTIR) spectroscopy and PXRD studies confirmed that this neutralization of the CNCs did not cause a significant change in the bulk composition of the CNC or the crystallinity. The improved dispersibility was attributed to the neutralization of the surface sulfate species causing decreased hydrogen bonding between the particles and increased solvent–particle hydrogen-bonding interactions. In general, cation-exchanged CNC-Xs are thermally more stable than their acidic counterparts, as discerned by TGA. Dispersions of CNC-Xs in polar organic solvents formed chiral nematic phases through EISA to give solid films with chiral photonic properties that were dependent on the initial CNC-X concentrations, as well as the size and hydrophobicity of the cations. An increasing cation size caused a blue-shift in the reflected color, while a red-shift was observed with increasing hydrophobicity of the alkylammonium cations, consistent with the results with aqueous CNC-X dispersions.

The authors demonstrated, furthermore, the successful formation of photonic polymer composite films by mixing CNC-X dispersions in DMF with soluble polymers such as polystyrene (PS), poly(methyl methacrylate) (PMMA), polycarbonate (PC), and poly(9-vinylcarbazole) (PVK). Slow evaporation of the solvent under a flow of dry air gave rise to iridescent composite films (Figure 6c) with a homogeneous chiral nematic structure, as proven by SEM (Figure 6d). The use of dry conditions was crucial to prevent phase separation of the polymer and the CNC suspension. The wavelengths of the reflection maxima of the films prepared with various polymers ranged from about 500 nm for PC to about 800 nm for PS, thus suggesting a pronounced effect of the hydrophobicity of the polymers on the EISA of the CNCs. The pitch of the chiral nematic structure and the reflected color could be further tuned by the addition of salts or variation of the polymer/CNC ratio. Significantly, this discovery paved the way to synthesize chiral nematic composite materials with polymers that are incompatible with aqueous CNC suspensions.

In the case of materials incorporating two organic substances with similar characteristics (CNC and the polymer), selective removal of one becomes challenging. However, removal of the template introduces mesoporosity—a desirable property that expands the range of potential applications for these materials. Khan et al. recently reported on novel phenol-formaldehyde (PF) resins, where removal of the template with retention of the chiral nematic order of the mesoporous polymer films was demonstrated. Mixing aqueous CNC suspensions (3–5 wt% at pH 2.4–6.9) with water-soluble PF, melamine-urea-formaldehyde (MUF), or urea-formaldehyde (UF) precursors yielded freestanding composite films with chiral nematic order after drying under ambient conditions.[64,93] The films have tunable colors ranging from UV to the near-IR, and some are highly flexible. Thermal curing was applied to enhance the cross-linking of the resin to obtain tough but brittle thermosetting composite films. The PF resins show significant mesoporosity, high mechanical flexibility, and fascinating tunable photonic properties upon removal of the CNCs.[93a] Selective removal of the CNC templates was achieved by treating the composite film with 16 wt% aqueous NaOH solution at 70 °C for 8–12 h. This treatment removed 85–90% of the CNCs from the polymer matrix, as confirmed by FTIR, solid-state NMR spectroscopy, and TGA, which resulted in mesoporous chiral nematic resins. Although the composite films are brittle, the mesoporous resin films are very flexible, with tensile strengths as high as 89 MPa and more than 4.5% elongation at failure. Samples dried from ethanol by supercritical CO_2 showed BET surface areas and pore volumes of 310–365 $m^2 g^{-1}$ and 0.5–0.7 $cm^3 g^{-1}$, respectively. The calculated BJH pore diameter is around 7 nm, which is close to the diameter of the individual CNCs that were removed from the composite. SEM revealed

Table 1: Properties of some mesoporous materials derived from CNC templating.

Materials	BET surface area [$m^2 g^{-1}$]	Avg. pore diameter [nm]	Thermal stability	Highlight	Ref.
silica	300–800	3.5–4.0	550 °C		[42, 75]
organo-silica	400–500	8.0–9.0		improved mechanical properties	[77]
titania	150–230	2.5–7.9	600 °C		[94]
carbon	578–1465	ca. 2.9	900 °C	freestanding films	[80]
polymer	310–365	ca. 7.0	ca. 300 °C	highly flexible	[93a]
MPC	ca. 250	ca. 8.0	ca. 300 °C	highly flexible	[93b]

that the chiral nematic structure can be efficiently embedded into the resin matrix by CNC templating, with the organization retained even after removal of the template.

CNCs were utilized as a sacrificial LC template in all the recent developments in synthesizing mesoporous photonic materials with chiral nematic structures. In contrast to this conventional approach, Giese et al. constructed mesoporous photonic cellulose (MPC) films from a conceptually new supramolecular co-templating method that was a serendipitous discovery.[93b] MPC can be derived from a two-step synthesis. In the first step, chiral nematic composite films of CNCs and UF resin (CNC-UF) are synthesized by self-assembly of aqueous CNC dispersions in the presence of a UF precursor through the typical EISA approach. After heat-curing, the composite films are treated with 15% aqueous KOH solution at 70 °C to remove the template. Surprisingly, however, it was found that alkaline treatment simultaneously removes the UF co-template and desulfates the CNCs. The cellulosic MPC material retains the original nanostructure of the composite, but now has mesoporosity, high flexibility, and an improved stability towards water. Removal of the UF resin and retention of the CNCs were confirmed with FTIR, solid-state NMR spectroscopy, PXRD, and EA. Nitrogen adsorption analysis showed that the MPC dried with supercritical CO_2 has a BET surface area and pore volume as high as 250 $m^2 g^{-1}$ and 0.6 $cm^3 g^{-1}$, respectively, with a BJH pore size centered near 8 nm. The absence of sulfate ester groups prevents the dispersion of MPC in polar solvents and contributes to its stability. It is notable that the alkaline treatment of composite films does not cause mercerization of cellulose, but it does reduce the crystallinity, which imparts increased flexibility to the MPC.

The collection of accessible inorganic and organic thin films based on cellulose templating serves as a platform for functional materials. Although the composite materials already show great photonic properties, because of their imprinted microstructure, the introduction of mesoporosity (Table 1) in conjunction with chiral nematic ordering might be useful for the accommodation of guests. Scheme 3 gives an overview of the different synthetic strategies presented herein and the resulting materials.

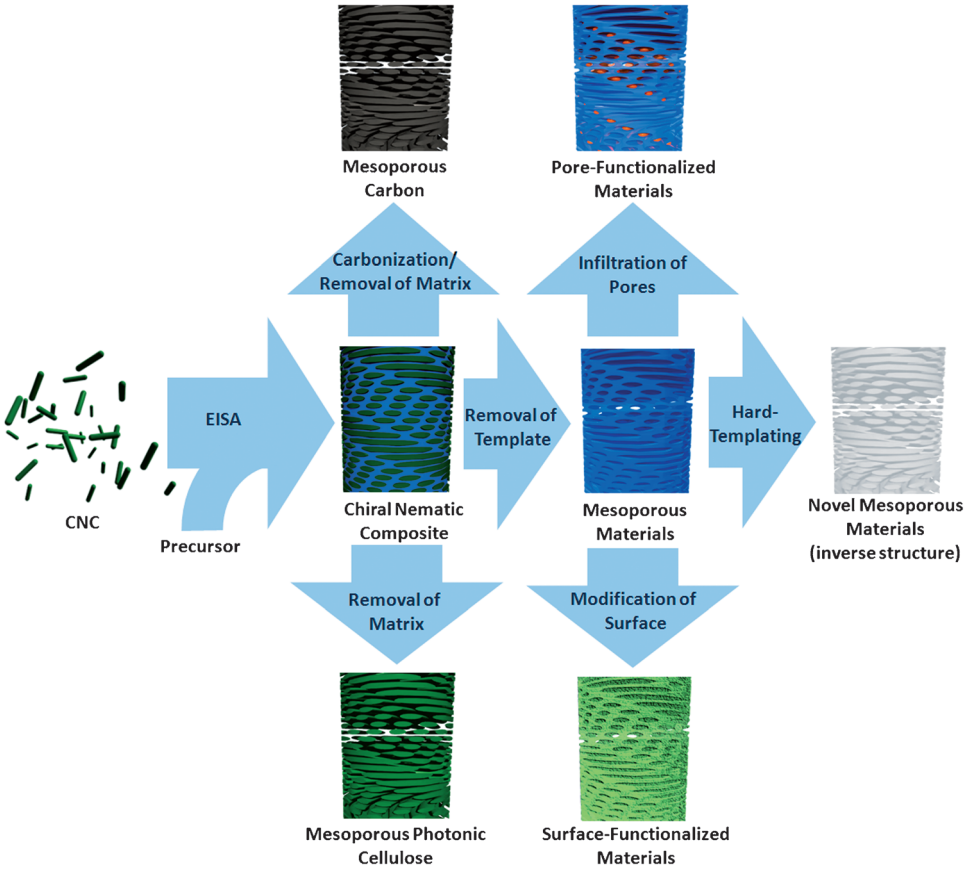

Scheme 3. Synthetic route to new nanostructured materials with chiral nematic order. In the presence of a suitable precursor, CNCs form a composite material upon EISA. Removal of the template leaves a mesoporous material which can be functionalized by infiltration of the pores, modification of the surface, or used as a hard template. Alternatively, carbonization followed by removal of silica yields chiral nematic mesoporous carbon, or removal of the matrix of the composite results in mesoporous photonic cellulose (MPC) films.

4. Functional Materials and Applications

The focus of this section is on CNC-templated materials, since these have been investigated intensively towards applications. As the number of materials based on or reinforced by CNCs is huge, the main aim of this Review is to summarize the recent progress in the development of new functional materials that make use of the chiral nematic order introduced by CNCs. The most remarkable feature of the described materials is their nanostructure, which causes impressive coloration because of the selective reflection of circularly polarized light. Structural coloration is ubiquitous in nature. A number of fossils and minerals as well as animals and plants have vibrant colors as a result of hierarchical organization, and even examples of tunable structural colorations are found. The reasons for this play of colors in nature (e.g. mimicry, signaling, mate choice, or camouflage) are not always fully understood.[95]

However, coloration as a result of diffraction from nanoscale structures has been inspiring materials chemists for decades. Structural coloration has the possibility to produce exciting colors that can be tuned, will not fade, and do not require toxic dyes.[96] By choosing suitable conditions for CNC templating, the chiral nematic order of the LLC phase can be imprinted into new materials (Figure 7 a–c).

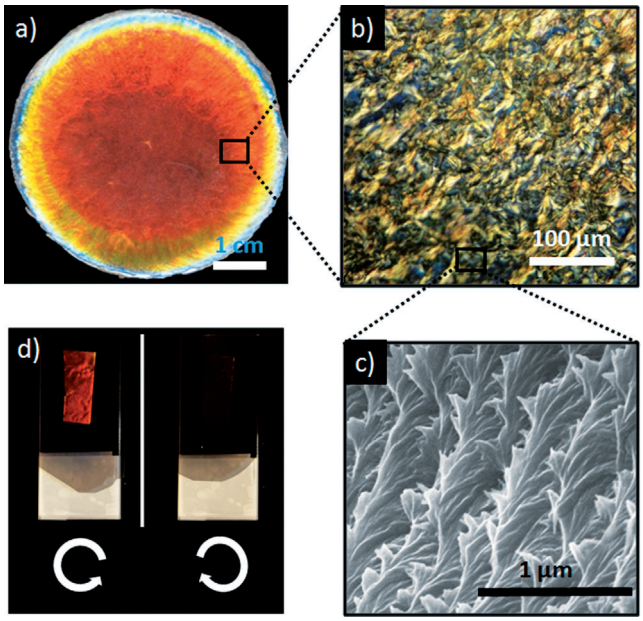

Figure 7. a) Optical characterization of the materials with chiral nematic structure that show vibrant iridescence; b) birefringence under crossed polarizers; c) twisted layers on the nanoscale level; d) a representative sample of a photonic polymer under left- and right-handed polarizers. Reproduced and adapted with permission from the American Chemical Society and John Wiley and Sons.[64,93a]

The transfer of the nanoscopic helicoidal ordering to materials such as glasses, ceramics, or polymers results in functional materials with potential applications in sensing, catalysis, and optoelectronic devices. Thus, the structure of the materials can be used in different ways with respect to functionality and application. First, the color of the material can be tuned by either changing the refractive index or the helical pitch of the chiral nematic structure (Figure 8). This allows the use of these materials in applications such as selective optical filters or in novel display devices. Second, the driving force for the change in color can be detected, thereby allowing the development of new sensors. As a consequence of the unique structure of these materials, both UV/Vis and CD spectroscopy are suitable for detecting the changes. Moreover, the mesoporous materials are capable of hard templating, thus allowing the transfer of the chiral nematic structure to otherwise inaccessible nanostructured materials. In addition to the use of the chiral nematic structure for sensing or nanocasting, surface modification of the materials and incorporation of functional guests (e.g. nanoparticles, quantum dots, or polymers) leads to novel applications that can take advantage of the mesoporous nature and chirality of the host materials.

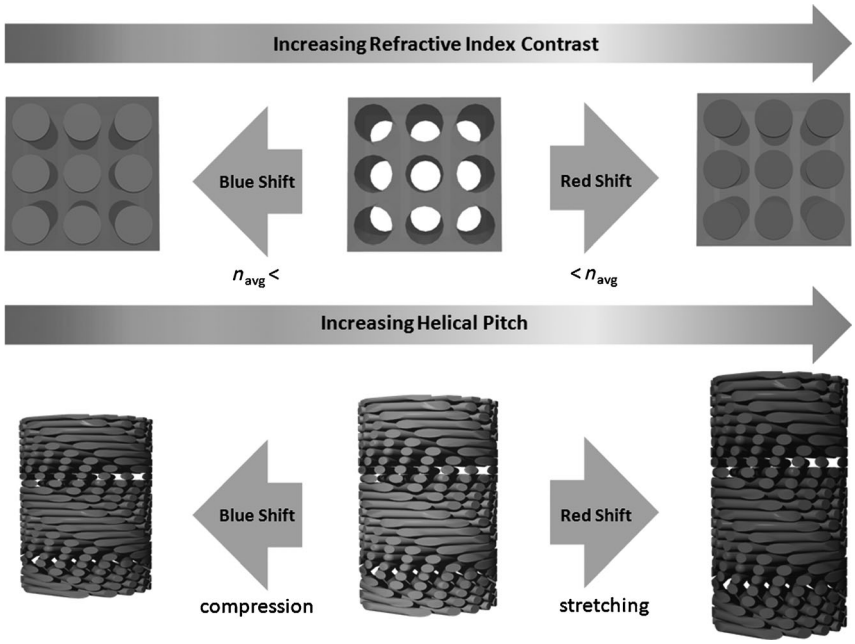

Figure 8. Postsynthetic manipulation of the optical properties of the photonic materials with chiral nematic order by addressing either the refractive index contrast or the helical pitch. Vice-versa, the driving force for the change in the optical properties can be used for sensing by following the UV/Vis or CD signals.

While the previous sections dealt with the synthesis and general properties of the materials derived from LC templating with CNCs and other cellulose derivatives, this section focuses on the modifications and potential future applications of these new materials.

4.1. Functionality by Tuning the Refractive Index

In 2010 and 2012, mesoporous silica and organosilica films were reported by Shopsowitz et al.[42,77] The chiral nematic structure of these materials leads to brilliant colors spanning from the UV to the near-IR region of the electromagnetic spectrum. As a result of the rigidity of the silica and organosilica networks, their structures—and therefore their colors—are locked in place after synthesis. These materials have no crystallinity, but rather they show birefringence that arises from the organization of the pores, which originates from the chiral nematic order of the template CNCs.[97] A unique property of chiral nematic mesoporous silica films that results from the birefringence is their change in optical properties upon infiltration of the pores with isotropic liquids. Water, for example, is rapidly absorbed and leads to completely transparent films with quenching of the colorful iridescence (Figure 9a). This effect is attributed to the approximate matching of the refractive index between the absorbed liquid in the pores (H_2O: $n = 1.33$) and the mesoporous silica (SiO_2: $n = 1.46$),[98] and is similar to responses observed for inverse opal photonic crystals.[99] Although the reflectance is completely extinguished to the naked eye, the small contrast in the refractive indices leads to a slightly red-shifted residual signal in the CD spectra (Figure 9b). Infiltration of the pores with solvents matching the refractive index of silica more closely (e.g. isopropanol: $n = 1.38$) leads to a stronger red shift and, for DMSO ($n = 1.48$), a complete elimination of the CD signal. It was demonstrated that thin films of chiral nematic mesoporous silica could be used to sense changes in the refractive index of aqueous sucrose solutions, by taking advantage of the changes in the CD signal.[75] These infiltration experiments demonstrate the suitability of the mesoporous silica and organosilica materials for sensing by following the UV/Vis or the CD signal, where the latter is more sensitive and can be used even when the color of the solutions is dominated by a strongly absorbing dye.

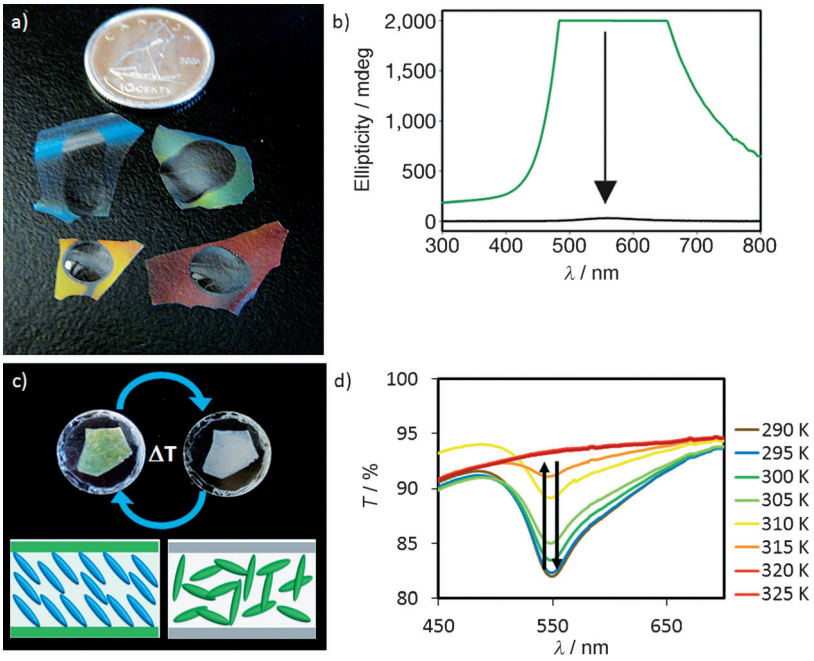

Figure 9. a) Photograph of the chiral nematic mesoporous silica films that lose their iridescence as a result of infiltration by water; b) the corresponding CD spectra before (green) and after (black) immersing the films in water; c) photograph of the thermochromic *n*-octyl-functionalized organosilica films infiltrated by 8CB at room temperature (left) and at 41 °C; d) the UV/Vis spectra showing the decreasing signal with rising temperature. Reproduced and adapted with permission from Nature Publishing Group and the American Chemical Society.[42,79]

In 2013, Giese et al. incorporated thermotropic liquid crystals into chiral nematic mesoporous materials to produce composite structures that show a temperature-dependent thermal switching of the reflection.[79] To control the color of these materials, the pores of the *n*-octyl-functionalized organosilica films were infiltrated with 4-cyano-4′-octylbiphenyl (8CB), a liquid crystal that shows large changes in orientation and refractive index in response to external stimuli.[100] The 8CB-loaded composite showed green iridescence (Figure 9c) at room temperature. Heating to the phase transition temperature of 8CB (from nematic to isotropic at 41 °C) resulted in the UV/Vis signal being gradually extinguished (Figure 9d), and finally giving an opaque gray sample at 50 °C. The process is reversible, with a small hysteresis effect observed through the heating/cooling cycles. To understand the color change of the materials on a molecular level, a ^{15}N-labeled analogue of the 8CB (^{15}N-8CB) was synthesized, injected into the pores of the *n*-octyl-functionalized organosilica films, and investigated by variable-temperature ^{15}N solid-state NMR spectroscopy, a powerful tool to investigate the molecular dynamics of liquid-crystalline phase transitions. The spectra showed broad signals at 21 °C that indicated the ^{15}N-8CB mesogens were aligned with the pores in their liquid-crystalline state. In contrast, the signals collapsed to a very sharp peak when heated to the isotropic state. These results support the assertion that the change in color mainly originates from a change in the refractive index caused by the alignment of the liquid crystals inside the pores. It is interesting to use the response of the encapsulated guest to affect the optical properties that arise primarily from the host. The reversible thermochromic response of the composites offers a new route to selectively tunable optical filters or temperature sensors.

4.2. Functionality by Tuning the Helical Pitch

A second way to control and modify the optical properties of the chiral nematic nanostructured materials is to address the pitch of the helical structure. This requires plastic or

elastic materials that can undergo compression or elongation without breaking. Hydrogels are a class of materials that undergo large dimensional changes when swollen in water. Not surprisingly, photonic hydrogels are highly interesting since they show large color changes in response to changes in the osmotic pressure and can function as sensors for analytes.[101] Although a small number of chiral nematic photonic hydrogels are known,[102] a general approach to a variety of functional hydrogels (e.g. for responding to changes in the pH value, temperature, or solvent polarity) is missing.[102] However, Kelly et al. recently reported a series of responsive photonic hydrogels based on CNCs (AAm, NIPAM, AAc, HEMa, PEGMa, bis, DiPEGMa) and proved their ability to sense changes in the polarity of solvents, pH value, or temperature.[65] The composite materials undergo fast and reversible swelling in water and other polar solvents. Swelling is accompanied by a significant red-shift in color by stretching the helical pitch of the chiral nematic organization of the composite materials. For example, the PAAm nanocomposite swells within 150 s and changes from a blue iridescent color into the near-IR region and becomes colorless. Immersing this hydrated film in pure ethanol rapidly leads to a blue-shift in the iridescence (Figure 10a). These hydrogels are, therefore, interesting as photonic alcohol sensors, since the increase in the ethanol content leads to a gradual blue-shift in both the UV/Vis and CD spectra. Interestingly, the synthesis of these hydrogels by photopolymerization allows latent images to be incorporated into the photonic hydrogel that only appear upon swelling. Increasing the irradiation time reduces the extent of swelling in a region, and it will show a smaller red-shift of its iridescence upon swelling. Figure 10b illustrates this concept, where masked regions (which are less photo-cross-linked) of a homogeneously iridescent dry photonic hydrogel swell the most in water until they reflect near-IR light.

By modifying the hydrogel composition it is possible to create tailor-made photonic hydrogels that respond to different stimuli. For example, polyacrylic acid/CNC hydrogels show a strong dependence on the pH value of the solution in which they are immersed, thus functioning as photonic pH sensors (Figure 10c). PNIPAm-CNC composites undergo a temperature-induced reversible blue-shift of about 40 nm upon reaching the lower critical solution temperature of 31 °C, which causes the swollen hydrophilic sample to become hydrophobic and contract.

Another way to introduce functionality in the chiral nematic hydrogels is by postsynthetic surface modification of the CNCs through cation exchange. The as-synthesized CNC–polymer composites bear acidic sulfate ester groups that readily undergo cation exchange upon neutralization of the gel in a dilute solution of base. After cation exchange by titration with sodium, ammonium, or tetraalkylammonium hydroxides, the nanocomposites show a significant change in their swelling behavior. All the composites exhibit an increased swelling ability in methanol, ethanol, acetone, and isopropanol as the size and hydrophobicity of the cations increase (Figure 10d). The simple cation exchange allows a variety of tailored photonic hydrogels to be prepared, and the postsynthetic modification is a promising approach to novel functional materials that cannot be obtained by the EISA method.

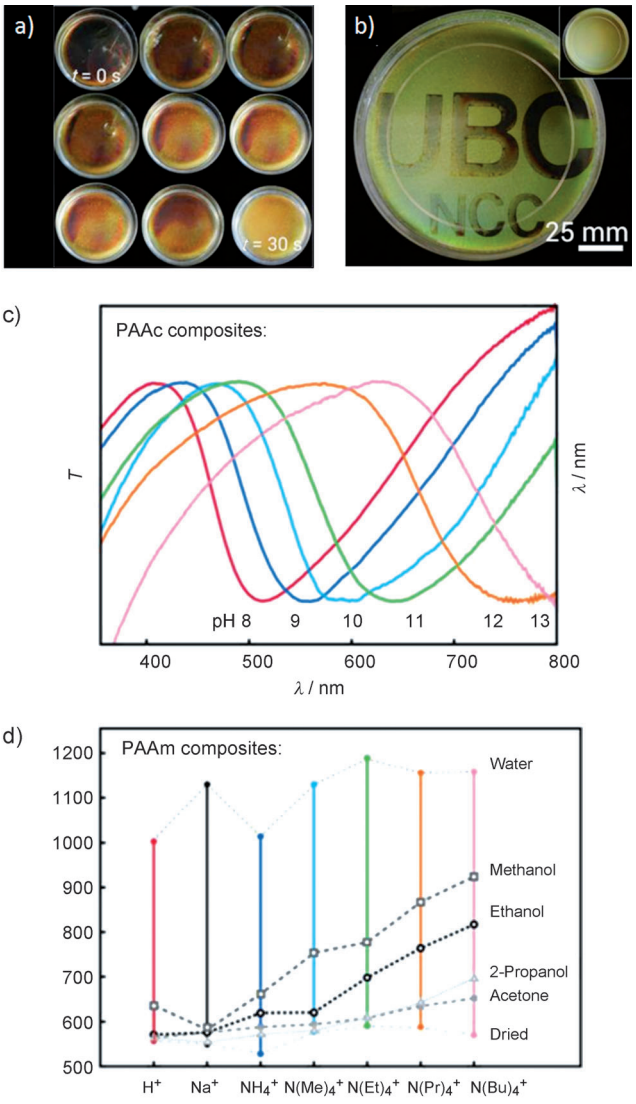

Figure 10. a) Images showing the deswelling of the nanocomposite hydrogels (66% CNC) in ethanol; b) photograph of a photopatterned iridescent hydrogel film revealing a latent image upon swelling of the dry film (inset) in water; c) transmission spectra showing the shifting reflection of the photonic CNC/PAAc hydrogel upon addition of base; d) graphical representation of the maximum reflected wavelength of cation-exchanged CNC/PAAm composites in a dry form and swollen in solvents. Reproduced and adapted with permission from John Wiley and Sons and the American Chemical Society.[65]

MUF-CNC composites show brilliant iridescent colors stemming from their chiral nematic structure.[64] An interesting feature of these materials is their high flexibility and capacity for color tuning by postsynthetic pressing. Samples with a high content of MUF polymer (40 wt%) appear slightly red or colorless because of a helical pitch within the near-IR region. Pressing the film leads to the pitch of the chiral nematic structure being reduced, thereby leading to a significant blue-shift in the reflected color. The change in the helical pitch is evident by UV/Vis and CD spectroscopy (Figure 11a) as well as by SEM. Once imprinted and finally

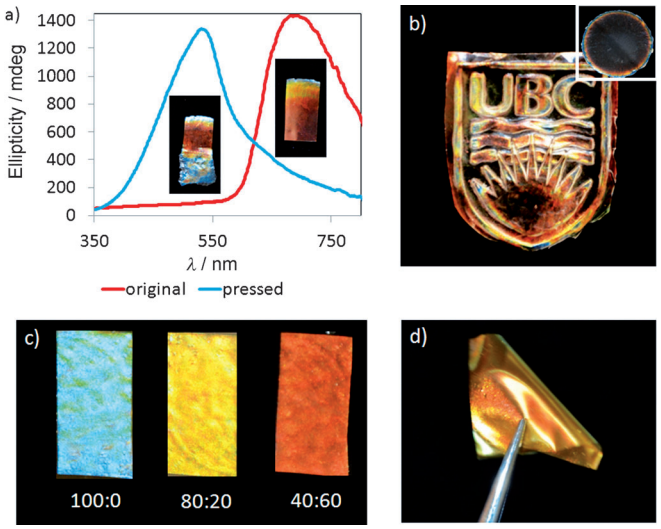

Figure 11. a) CD spectra and inserted photographs of the MUF/CNC composite stripes before and after pressing; b) photograph of a MUF-CNC composite with an imprinted photonic pattern, as obtained from the film shown in the inset; c) photograph of a mesoporous PF film after being immersed in different ratios of ethanol/water; d) a photograph of a mesoporous PF resin illustrates its high flexibility. Reproduced and adapted with permission from the American Chemical Society and John Wiley and Sons.[64,93a]

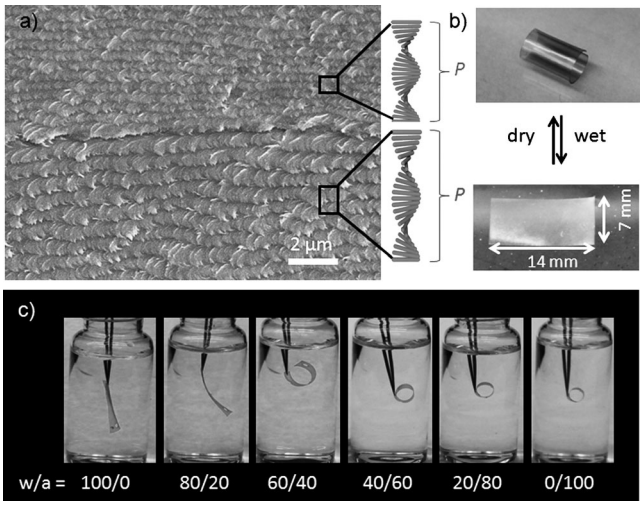

Figure 12. a) SEM image of a cross-section of the mesoporous polymer bilayer showing the different helical pitches of the layers; b) photographs of the curling and uncurling of the bilayered mesoporous polymer films upon alternately soaking in water and drying; c) photographs of the bilayer mesoporous polymer films in mixtures of water and acetone (w/a). Reproduced and adapted with permission from John Wiley and Sons.[103]

cured at 100 °C, the materials are locked and no further manipulation of the photonic pattern is possible. The postsynthetic modification of the photonic properties of the MUF samples allows the imprinting of colorful patterns (Figure 11 b), which might be a useful security feature for documents or currency.

In a similar way, mesoporous PF resins can be prepared by first forming chiral nematic PF-CNC composites, then extracting the CNC template.[93a] These materials show a superior swelling behavior as a result of their mesoporous structure and they change color within seconds by the swelling (in water) or de-swelling (in ethanol) of the helicoidal network. The films undergo a systematic color change when the proportion of ethanol in water is varied, a change that can easily be followed by the naked eye (Figure 11 c) and quantified by UV/Vis and CD spectroscopy. The very fast response of the samples to the polarity change of the solvent makes them interesting for sensing applications and, as a consequence of their high flexibility (Figure 11 d), they can be employed for the development of novel security features. The films show a very strong contrast when viewed under left- and right-handed circular polarizers (Figure 7 d).

It was possible to prepare bilayer mesoporous photonic PF resins by layer-by-layer deposition followed by removal of the CNC template.[103] The bilayer films have layers in which the chiral nematic structure has a different helical pitch and, consequently, reflect light at two different wavelengths. Furthermore, these materials show interesting actuator behavior. Whereas usual bilayered materials for actuation are obtained by the combination of an active layer on a substrate,[104] the bilayer mesoporous PF resins consist of two active layers of the same material that differ only in their nanostructures (Figure 12 a). The structural difference in the pore size and density between the two layers results in an asymmetric swelling behavior, which imparts actuator properties to these materials. Detailed swelling studies reveal that the layer of longer helical pitch and larger pore size swells more than the one with a shorter helical pitch. This leads to directional curling and uncurling upon drying and swelling in polar solvents. For example, a dry, curled sample uncurls gradually upon swelling in water within 10 s, while recurling in acetone takes 14 s with an insignificant mechanical fatigue (Figure 12 b,c). Thus, the response is much faster than earlier reports on HPC-based actuators[105] or polymer microgels that mimic muscles.[106] The reversible bending of the samples is assigned to the difference in the permeability of the individual layers and the consequent difference in the expansion or shrinkage of the bilayered chiral nematic structure that leads to a change in color. The fast dynamic mechanical and photonic response of the bilayered materials is the first example of a bilayer material with tunable photonic properties and might lead to novel applications in optics and soft robotics.

Alkaline treatment of UF-CNC resins led to removal of the UF resin, thereby leaving a chiral nematic mesoporous form of cellulose, MPC. MPC is mesoporous, thus allowing fast swelling in polar solvents and a rapid response (Figure 13 a–c) to changes in the polarity, which can easily be followed by the naked eye (Figure 13 b). In pure ethanol, the film appears deep blue with a maximum reflection wavelength at 430 nm. A successive increase of the water content red-shifts the color, finally reaching 840 nm in pure water. The approximately 400 nm shift of the signals in the UV/Vis and CD spectra (Figure 13 a) occurs within 10 s, thus making this material interesting for sensing applications. However, even more impressive is the high flexibility and piezochromic

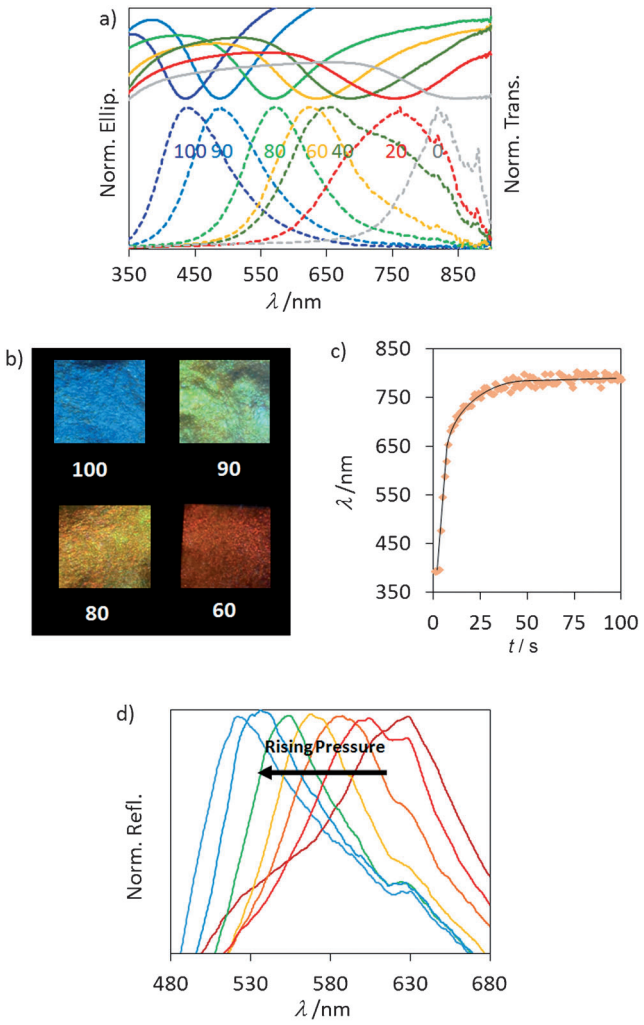

Figure 13. a) UV/Vis/CD data and b) photographs of samples of MPC immersed in mixtures of water and ethanol (the value indicates the % ethanol); c) swelling kinetics of MPC when immersed in water; d) reflectance spectra of water-swollen samples upon pressing. Reproduced and adapted with permission from John Wiley and Sons.[93b]

behavior of the water-swollen samples. When pressed, the structure experiences a reversible compression of the helical pitch, thereby leading to a highly visible blue shift of more than 100 nm (Figure 13d). Initially colorless samples (long pitch, reflecting near-IR light) can become visibly colored when compressed. The systematic blue-shift offers a novel route to sense pressure that depends on the chiral nematic structure of the MPC. It is interesting that as MPC is made only of cellulose, this is an original functional application of cellulose films.

4.3. Transfer of Chirality

Another interesting source of functionality in the chiral nematic materials, besides tuning the pitch or refractive index, is to transfer the chiral information to guests. Molecules, polymers, and nanoparticles can be encapsulated as guests within the mesopores of the chiral nematic structures. These hybrid materials have potential applications in catalysis, biosensing, and optoelectronic devices.

Hard templating has emerged as a powerful tool in materials chemistry for the synthesis of novel highly ordered materials such as photonic crystals.[107] The mesoporous host acts as template to transfer a nanostructured negative image to a second material, which resembles the initial mesophase used to template the host. After selective etching of the host template, a new nanostructured material is obtained. Hard templating allows nanostructured materials to be synthesized whose precursors are incompatible with the self-assembly of the LLC template.[108] For example, the hydrolysis kinetics of titanium(IV) precursors are generally too fast for them to be used in aqueous LLC templating strategies. Various approaches have been used over the past two decades to synthesize new mesoporous materials with diverse structures by hard templating.[10b,109]

In 2011, MacLachlan and co-workers reported the hard templating of chiral nematic mesoporous carbon (CNMC) films with BET surface areas as high as 1465 $m^2 g^{-1}$ (Figure 14a).[80] Previously, mesoporous carbon[110] was prepared

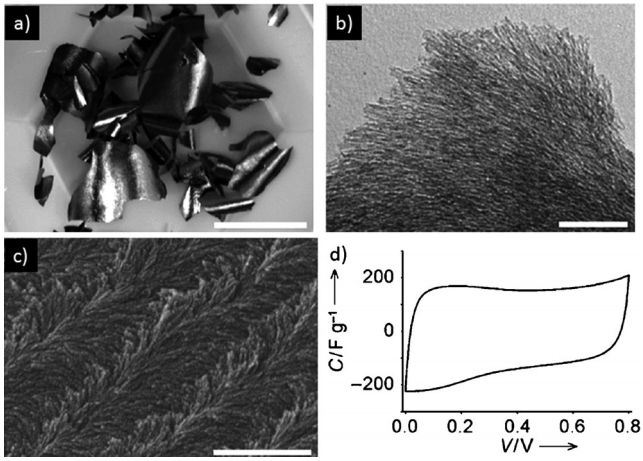

Figure 14. a) A photograph of a sample of the CNMC (scale bar: 2 cm); b) TEM image of CNMC (scale bar: 200 nm); c) SEM image of CNMC (scale bar: 500 nm); d) cyclic voltammogram of a symmetric capacitor setup in 1 M H_2SO_4 (scan rate = 2 $mV s^{-1}$). Reproduced and adapted with permission from John Wiley and Sons.[80]

by loading porous silica with a suitable carbon source, often sucrose, followed by carbonization and then removal of the silica template by etching. In contrast, chiral nematic mesoporous carbon was synthesized by an easier route that used the original CNC template as a carbon source. Thus, pyrolysis of a silica-CNC composite film in an inert atmosphere yielded highly ordered CNMC films with long-range chiral nematic order. SEM and TEM studies (Figure 14b,c) confirmed the chiral nematic structure of the carbon. Furthermore, the carbon itself was used as a template to hard-template silica, which was shown to be chiral nematic. Since mesoporous carbon is a promising material for applications in electrochemical capacitors, catalyst supports, and field-effect transistors,[110a,111] the electrochemical performance of the

CNMCs was investigated. Variable-temperature conductivity measurements showed that the carbon is semiconducting in the range 20–180 °C. In addition, the material was demonstrated to be an effective electrode for supercapacitors. A CNMC film was squeezed between two electrodes using 1 M H_2SO_4 as an electrolyte. The cyclic voltammogram (CV) shows a rectangular shape with a slight slope indicating Faradaic processes at the electrodes (Figure 14 d). However, the galvanostatic charging/discharging profile reveals near-ideal capacitor behavior, with a capacity of 170 $F g^{-1}$ at a current load of 230 $mA g^{-1}$. This performance is in good agreement with previously reported carbon materials.[112] Although the potential of the new CNMC films in applications such as electrochemical and energy storage devices was proven, the performance is not related to its chiral nematic structure. Further studies are needed to clarify the use of these materials in enantioselective catalysis as well as in electrochemical synthesis and sensing that might take advantage of their chirality.

As a proof-of-concept, Shopsowitz et al. utilized mesoporous silica as a hard template to synthesize chiral nematic titania.[94] Peptized $TiCl_4$ solutions are incompatible with aqueous CNC dispersions and form gels instantaneously after mixing, without forming a chiral nematic phase. However, repeated loading of a $TiCl_4$ solution into mesoporous chiral nematic silica films gives a silica–titania composite. Each cycle of loading was followed by drying at 80 °C and annealing at 200 °C. The resulting composite was then calcined at 600 °C and the silica support was removed by etching in 2 M NaOH to yield freestanding, mesoporous titania films. The iridescence characteristic of chiral nematic structures was circularly polarized exclusively in a left-handed manner, as evident when the samples were viewed under circular polarizers (Figure 15 a). Mesoporous titania with various pore diameters

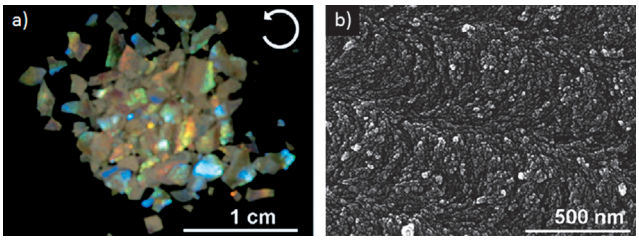

Figure 15. a) Photograph of chiral nematic titania films viewed under a left-handed circular polarizer; b) SEM image of the same films. Reproduced and adapted with permission from John Wiley and Sons.[94]

(2.5–7.9 nm), pore volumes (0.23–0.31 $cm^3 g^{-1}$) and surface areas (234–149 $m^2 g^{-1}$) can be synthesized by using silica films prepared either by calcination or acid extraction of CNCs. Replication of the helical chiral nematic structure in titania by the hard-templating approach was confirmed by SEM (Figure 15 b). PXRD analysis of the titania films showed that they are composed of nanocrystalline anatase instead of the thermodynamically favored rutile phase of bulk titania. Nanoconfinement during crystallization inside the mesopores of silica templates favored the formation of the anatase polymorph. Successful replication of the chiral nematic structure into titania by this hard-templating approach thus opened another synthetic route to prepare chiral nematic materials that were otherwise inaccessible by direct templating with CNCs. These new highly porous titania films are promising for applications in dye-sensitized solar cells, photocatalysts, sensors, and batteries. Bein and co-workers recently made mesoporous titania by using CNCs directly as a template, but did not observe any chirality.[113] They demonstrated that the porous material could be used for dye-sensitized solar cells and photovoltaic devices.

Just recently, Chu et al. reported a closely related hard-templating approach for chiral nematic zirconia (ZrO_2) and europium-doped zirconia films (ZrO_2/Eu^{3+}).[114] The films were obtained by repeated loading of chiral nematic mesoporous silica films with aqueous solutions of $ZrOCl_2$ or $ZrOCl_2/Eu(NO_3)_3$. Subsequent drying and calcination of the composite samples and final removal of the silica under basic aqueous conditions yielded the desired ZrO_2 and ZrO_2/Eu^{3+} films. Gas adsorption measurements revealed a mesoporous structure based on the BJH model with BET surface areas of 140–182 $m^2 g^{-1}$ and pore volumes of 0.27–0.31 $cm^3 g^{-1}$. The replication of the chiral nematic order of the original silica films was proven by SEM and CD spectra. PXRD analysis of both samples showed characteristic diffraction patterns for tetragonal ZrO_2, thus suggesting isostructural substitution of Eu^{3+} for Zr^{4+}. The ZrO_2/Eu^{3+} films showed the characteristic luminescence of the Eu^{3+} combined with the photonic properties transferred from the chiral nematic template. Interestingly, the decay time constants of the chiral nematic ZrO_2/Eu^{3+} samples are significantly higher than those of an achiral reference sample. This result is usually indicative of differences in the local environments of the Eu^{3+} ions.[115] However, in this case, XPS revealed no significant difference in the chemical environment of the two samples, so the authors attributed the deviation in luminescence to the chiral nematic order of the ZrO_2/Eu^{3+} sample.

The studies described above (with carbon, titania, and zirconia) have proven the suitability of chiral nematic mesoporous silica in the hard templating of solid-state materials that combine the benefit of luminescence, photonic properties, and mesoporosity. Driven by the successful hard templating of titania, a number of studies were undertaken to investigate the transfer and use of the chiral nematic order of the mesoporous silica materials with respect to novel functional hybrid materials. Qi et al. and Kelly et al. published the synthesis of mesoporous silica films decorated with metal nanoparticles (NPs).[116] Metal NPs are important for their bioactivity and catalytic activity, as well as for chemical sensing by making use of their surface plasmon resonance (SPR).[117] Controlling the supramolecular organization of metal NPs is crucial for taking full advantage of their properties. Metal NP assemblies within chiral nematic mesoporous silica showed a CD signal assigned to the SPR that arises from the helical organization of the particles. It was notable that, prior to this, chirality was only induced to metal NPs by coordination of chiral ligands, and it was debatable whether chiral organizations of metal NPs could display CD signals.[118]

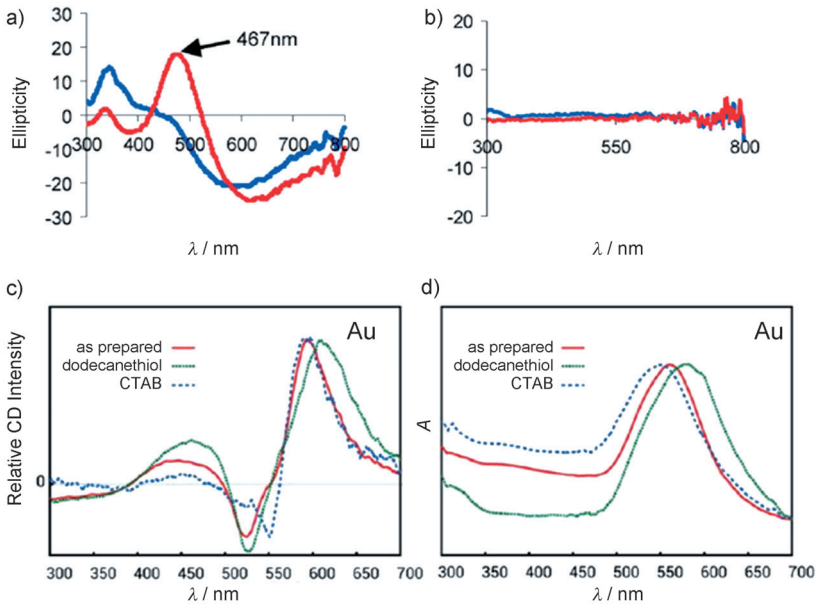

Figure 16. a) CD spectra of chiral nematic mesoporous silica films doped with silver NPs; b) CD spectra of achiral mesoporous silica films doped with silver NPs (blue before and red after soaking with water); c) CD and d) UV/Vis spectra of chiral nematic silica films doped with gold NPs, showing the changes upon immersion of the samples in solutions containing dodecanethiol and CTAB. Reproduced and adapted with permission from the American Chemical Society.[116]

To prove that the chiral nematic structure of the porous silica can induce chirality to metal NP assemblies, silica films with silver, gold, and platinum NPs were synthesized by two different approaches: in situ and postsynthetic. In the first method, silver NPs were synthesized inside the pores of the mesoporous silica films, while in the second one small quantities of the NP precursors were added to the CNC/silica gel and co-organized with the silica and CNC during EISA. Detailed CD studies revealed that the optical activity of the SPR signal solely arises from the chiral nematic long-range order of the chiral nematic silica host (Figure 16a,b). As the SPR of metal NPs is highly sensitive to surface binding events, these materials are interesting for sensing biomolecules (such as DNA or proteins) or heavy metal ions.[119] To investigate the sensing performance of the chiral nematic NP/silica hybrids, dodecanethiol and cetyltrimethylammonium bromide (CTAB) were tested as model compounds. The CD spectra (Figure 16c) show red-shifts for the negative signal of the CTAB (ca. 25 nm) and for the positive signal of the dodecanethiol (ca. 15 nm). In contrast, the absorption spectra (Figure 16d) for the mesoporous silica films functionalized with gold NPs show a red-shift for the dodecanethiol, while the CTAB leads to a blue-shift. These simple experiments show that slight changes in the local environment of the chiral nanoaggregates lead to a significant change in their CD and absorption spectra and show their suitability for biosensing. These hybrid nanomaterials are also interesting for catalysis.

Another area of growing interest in functional materials is the fabrication of quantum dot (QD) hybrid materials.[120] Combining the optical properties of photonic crystals with the electronic characteristics of semiconducting QDs might lead to novel functional materials with applications in optoelectronics, sensing, optical amplifiers, or lasers.[121] In 2013, Nguyen et al. reported the first LC-templated hybrid material by marrying the iridescence of the chiral nematic silica (Figure 17a) with the luminescence of CdS QDs (Figure 17b).[122] The synthesis of these materials required a careful balance of the surface coatings of the QDs to retain the luminescence of the QDs and to permit chiral nematic order of the CNCs. In addition, controlled calcination of the composite films was required to maintain the QD integrity and remove the CNC template. Once the correct conditions were applied, it was possible to prepare chiral nematic mesoporous silica with embedded QDs. The materials show the characteristic luminescence of the QDs and iridescence of the chiral nematic mesoporous silica host. The luminescence lifetimes before and after calcination are 1.55 and 1.75 ns, respectively, in agreement with related materials,[123] and verify the retention of the luminescence after calcination (Figure 17c).

To investigate the capability of the hybrid materials for practical applications, the quenching of the QD luminescence by solutions and vapors of 2,4,6-trinitrotoluene (TNT) was studied. Immersing a CdS-doped silica film in a 5.5×10^{-3} mM solution of TNT in toluene led to a complete loss of luminescence. The quenching arises from electron transfer from the CdS QDs to the electron-deficient π system of the TNT.[124] The quenching is reversible and luminescence recovers after removal from the TNT solution. Exposure of the CdS/silica films to TNT vapors leads to a gradual decrease in the emission intensity, reaching a steady-state value after 10 min with a quenching efficiency of 30% (Figure 17d). This value is in good agreement with the establishment of the donor–acceptor complex equilibrium. The high porosity and the excellent stability of the new CdS/silica hybrids guarantee a high accessibility of the QDs, which may make them attractive for incorporation into sensors for explosives.[125]

In a similar way, composite materials of chiral nematic mesoporous organosilica and poly(*p*-phenylenevinylene) (PPV) were employed in 2013 to sense TNT.[126] PPV is a conjugated organic polymer that has attracted considerable attention for use in a number of applications in organic electronics,[127] lasers,[128] sensing,[129] and nanocomposites.[130] A crucial factor in most of the applications based on conjugated polymers is their alignment and organization to enhance their electrochemical and optical performance.[131] Mehr et al.[126] investigated the organization of PPV inside the pores of chiral nematic organosilica films. The PPV was formed by a surface-activated polymerization within the channels of the silica. The obtained hybrid materials are still mesoporous and combine the iridescence arising from the chiral nematic host and the luminescence of PPV (Figure 18a). CD spectroscopic investigations prove the transfer of the chiral nematic structure from the host to the conjugated

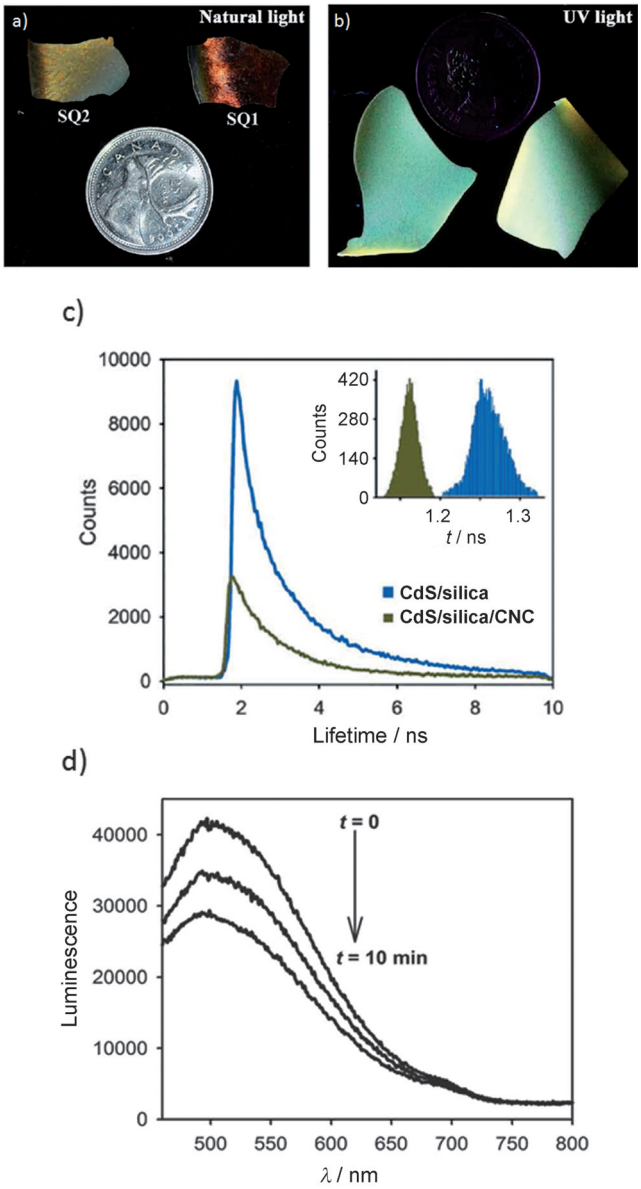

Figure 17. a) Photographs of the chiral nematic silica films doped with CdS QDs showing the characteristic iridescence of the host material under natural light; b) luminescence of the QDs evident under UV light; c) lifetime decay curves for the luminescence of CdS/silica/CNC composites and CdS/silica hybrid materials; d) time-dependent decay of the luminescence of CdS/silica upon exposure to TNT vapors. Reproduced and adapted with permission from John Wiley and Sons.[122]

polymer through the appearance of a new signal around 430 nm. To demonstrate a potential application for the composite materials, they were immersed in a solution of TNT in ethanol and their luminescence was monitored. The characteristic luminescence of PPV is immediately quenched and the films appear slightly red iridescent. The quenching can be followed by the naked eye under irradiation with UV light (Figure 18a,b). After washing the samples with ethanol, the fluorescence is nearly completely recovered (Figure 18c). Although the reversible quenching of the fluorescence can easily be observed by luminescence spectroscopy, the CD

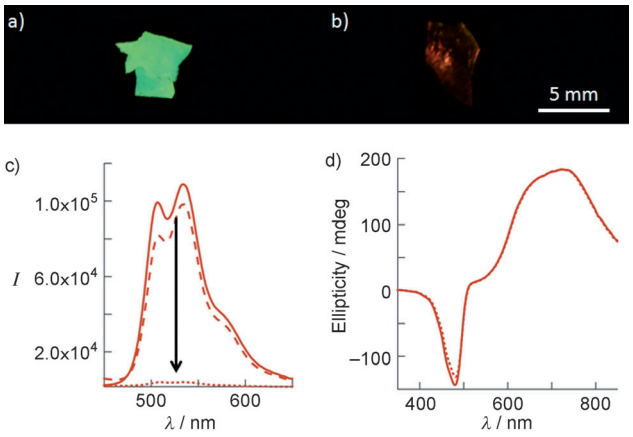

Figure 18. a) Photographs of chiral nematic PPV/organosilica composite films viewed under natural light and b) under UV light; c) fluorescence quenching of a sample upon exposure to a solution of TNT in ethanol; arrow: decreased emission intensity upon exposure to TNT; d) the CD spectra before and after the luminescence quenching are identical. Reproduced and adapted with permission from the American Chemical Society.[126]

signal (Figure 18d) shows no significant change, thereby proving that the optical change is exclusively assigned to fluorescence resonance energy transfer from the excited state of the conjugated polymer to TNT.

It should be noted that the functionality of the CdS QDs and the PPV-doped organosilica films does not take advantage of the chiral nematic structure, but rather relies on the mesoporosity and the freestanding nature of the films. Nevertheless, these experiments demonstrate that the luminophores in these hybrid materials are accessible to analytes and might be useful in sensing and optoelectronic applications. Further detailed studies are required to prove the solution and gas-phase sensing ability of these materials.

5. Conclusion and Outlook

In this Review, we have tried to show that cellulose and its derivatives are excellent liquid-crystalline templates for accessing diverse new porous materials with interesting structures. Readily available, sustainable, and nontoxic, cellulose is an inexpensive template that is amenable to commercial-scale applications. HPC and EC have potential application in templating materials with novel structures, but cellulose nanocrystals have emerged as the champion cellulose-based template material. The fast self-assembly of CNCs is compatible with many inorganic precursors and provides a perfect base for sol–gel reactions. The chirality could be transferred to several inorganic replicas and was maintained even after removal of the organic template to introduce porosity. Freestanding films of silica and other materials templated by CNCs show interesting properties, including tunable pore sizes, controllable surface chemistry, and a chiral nematic arrangement of pores that imparts tunable photonic properties to the materials. The incorporation of guests into the chiral mesopores further expands the field of accessible functional materials.

The future of chiral nematic materials templated by cellulose, especially CNCs, is bright and iridescent. These new materials offer a host of exciting directions for both pure and applied research. In terms of applications, the first steps towards using cellulose-templated materials as reflectors, polarizers, electrode materials, photocatalysts, and sensors have been demonstrated in proof-of-principle experiments, but significant technical developments are required before these materials can be commercialized. The presented materials show great potential in sensing, catalysis, separation membranes, security features, capacitors, actuators, and as hard templates themselves. Many fundamental studies remain to understand these materials: How do they form? How do substances behave in the chiral channels? Is there imprinted chirality on multiple length scales in these materials? Can the methods of templating silica and organosilica be extended to more exotic materials, such as semiconductors? Is it possible to achieve enantioselective adsorption or catalysis within the chiral channels? There are many new opportunities for researchers interested in pursuing the science of chiral nematic mesoporous materials—a new area of research with a twist.

Abbreviations

(E-CE)C	ethylcyanoethylcellulose
8CB	4-cyano-4′-octylbiphenyl
AAc	acrylic acid
AAm	acrylamide
avg	average
BET	Brunauer–Emmett–Teller
bis	*N*,*N*′-methylenebisacrylamide
BJH	Barrett–Joyner–Halenda
CD	circular dichroism
CNC	cellulose nanocrystal
CNC-H	acidic form of CNCs
CNC-X	salt form of CNCs (X = cation)
CNMC	chiral nematic mesoporous carbon
CP/MAS	cross-polarization magic-angle spinning
CTAB	cetyltrimethylammonium bromide
CV	cyclic voltammogram
DiPEGMa	polyethylene glycol dimethacrylate
DMF	dimethylformamide
DMSO	dimethylsulfoxide
DVB	divinylbenzene
EC	ethyl cellulose
EDX	energy-dispersive X-ray analysis
EISA	evaporation-induced self-assembly
FTIR	Fourier-transform infrared
HEMa	2-hydroxyethyl methacrylate
HIM	helium ion microscopy
HPC	hydroxypropylcellulose
LbL	layer-by-layer
LC	liquid crystal
LLC	lyotropic liquid crystal
LLD	luminescence lifetime decays
MPTOS	3-(methacryloyloxy)propyltrimethoxysilane
MUF	melamine urea formaldehyde
n	refractive index
NCh	nanocrystalline chitin
NIPAm	*N*-isopropylacrylamide
NMF	*N*-methylformamide
NMR	nuclear magnetic resonance
NP	nanoparticle
P	helical pitch
PC	polycarbonate
PEGMa	polyethylene glycol methacrylate
PF	phenol formaldehyde
PHEMA	poly(2-hydroxyethyl methacrylate)
PMMA	poly(methyl methacrylate)
MPC	mesoporous photonic cellulose
POM	polarized optical microscopy
PPV	poly(*p*-phenylenevinylene)
PS	polystyrene
PVK	poly(9-vinylcarbazole)
PXRD	powder X-ray diffraction
QD	quantum dot
SEM	scanning electron microscopy
SPR	surface plasmon resonance
TEM	transmission electron microscopy
TEOS	tetraethyl orthosilicate
TGA	thermogravimetric analysis
TMOS	tetramethyl orthosilicate
TNT	2,4,6-trinitrotoluene
Tyzor-LA	titanium(IV) bis(ammonium lactate) dihydroxide
UF	urea formaldehyde
WAXS	wide-angle X-ray scattering

We are grateful to NSERC, FPInnovations, ArboraNano, NORAM, and CelluForce for generous funding of this work. M.G. and L.K.B. thank the DAAD and the Humboldt Foundation, respectively, for postdoctoral fellowships. We wish to thank all of our past and present co-workers who have contributed to the work discussed in this Review; most of their names appear in the citations. Finally, we are sincerely indebted to our collaborators and friends, Wadood Hamad and Richard Berry, who introduced us to CNCs and have been very supportive of our work since the beginning.

Received: July 12, 2014
Published online: December 17, 2014

[1] W. Lu, C. M. Lieber, *Nat. Mater.* **2007**, *6*, 841 – 850.
[2] Y. Fang, B. M. Phillips, K. Askar, B. Choi, P. Jiang, B. Jiang, *J. Mater. Chem. C* **2013**, *1*, 6031 – 6047.
[3] E. Burstein, M. L. Cohen, D. L. Mills, P. J. Stiles, *Nanomagnetism*: *Ultrathin Films*, *Multilayers and Nanostructures*, Elsevier, London, **2006**.
[4] Q. Zhang, E. Uchaker, S. L. Candelaria, G. Cao, *Chem. Soc. Rev.* **2013**, *42*, 3127 – 3171.
[5] a) J. Wang, *Electroanalysis* **2005**, *17*, 7 – 14; b) J. J. Gooding, *Electrochim. Acta* **2005**, *50*, 3049 – 3060.
[6] A. Huczko, *Appl. Phys. A* **2000**, *70*, 365 – 376.
[7] a) P. D. H.-G. Rubahn, *Basics of Nanotechnology*, Wiley-VCH, Weinheim, **2008**; b) G. A. Ozin, *Adv. Mater.* **1992**, *4*, 612 – 649.
[8] Y. S. Lee, *Self-Assembly and Nanotechnology*: *A Force Balance Approach*, Wiley, Hoboken, **2008**.

[9] K. Zhu, J. Sun, H. Zhang, J. Liu, Y. Wang, *J. Nat. Gas Chem.* **2012**, *21*, 215 – 232.
[10] a) L. F. Giraldo, B. L. López, L. Pérez, S. Urrego, L. Sierra, M. Mesa, *Macromol. Symp.* **2007**, *258*, 129 – 141; b) A. Thomas, F. Goettmann, M. Antonietti, *Chem. Mater.* **2008**, *20*, 738 – 755.
[11] N. Pal, A. Bhaumik, *Adv. Colloid Interface Sci.* **2013**, *189 – 190*, 21 – 41.
[12] a) D. Papapostolou, S. Howorka, *Mol. BioSyst.* **2009**, *5*, 723 – 732; b) S. Che, Z. Liu, T. Ohsuna, K. Sakamoto, O. Terasaki, T. Tatsumi, *Nature* **2004**, *429*, 281 – 284; c) B. Liu, Y. Yao, S. Che, *Angew. Chem. Int. Ed.* **2013**, *52*, 14186 – 14190; *Angew. Chem.* **2013**, *125*, 14436 – 14440; d) Z. Huang, Y. Yao, S. Che, *Chem. Eur. J.* **2014**, *20*, 3273 – 3276; e) Y. Yao, D. Wang, L. Han, S. Che, *Chem. Eur. J.* **2013**, *19*, 15489 – 15492.
[13] a) D. G. Shchukin, A. A. Yaremchenko, M. G. S. Ferreira, V. V. Kharton, *Chem. Mater.* **2005**, *17*, 5124 – 5129; b) T.-Y. Ma, L. Liu, Z.-Y. Yuan, *Chem. Soc. Rev.* **2013**, *42*, 3977 – 4003.
[14] a) C. G. Göltner, M. Antonietti, *Adv. Mater.* **1997**, *9*, 431 – 436; b) L. Han, S. Che, *Chem. Soc. Rev.* **2013**, *42*, 3740 – 3752; c) B. J. Melde, B. T. Holland, C. F. Blanford, A. Stein, *Chem. Mater.* **1999**, *11*, 3302 – 3308; d) Q. Huo, D. I. Margolese, G. D. Stucky, *Chem. Mater.* **1996**, *8*, 1147 – 1160; e) H. Yang, N. Coombs, I. Sokolov, G. A. Ozin, *Nature* **1996**, *381*, 589 – 592; f) G. S. Attard, J. C. Glyde, C. G. Göltner, *Nature* **1995**, *378*, 366 – 368.
[15] G. A. Jeffrey, *Acc. Chem. Res.* **1986**, *19*, 168 – 173.
[16] R. Dabrowski, P. Kula, J. Herman, *Crystals* **2013**, *3*, 443 – 482.
[17] G. J. T. Tiddy, *Phys. Rep.* **1980**, *57*, 1 – 46.
[18] A. M. Donald, A. H. Windle, S. Hanna, *Liquid Crystalline Polymers*, Cambridge University Press, Cambridge, **2006**.
[19] a) I. W. Hamley, *Soft Matter* **2010**, *6*, 1863 – 1871; b) T. Z. Rizvi, *J. Mol. Liq.* **2003**, *106*, 43 – 53.
[20] a) F. C. Bawden, N. W. Pirie, J. D. Bernal, I. Fankuchen, *Nature* **1936**, *138*, 1051 – 1052; b) Z. Dogic, S. Fraden, *Phys. Rev. Lett.* **1997**, *78*, 2417 – 2420; c) Z. Dogic, S. Fraden, *Langmuir* **2000**, *16*, 7820 – 7824; d) S.-W. Lee, B. M. Wood, A. M. Belcher, *Langmuir* **2003**, *19*, 1592 – 1598.
[21] I. Dierking, *Textures of Liquid Crystals*, Wiley-VCH, Weinheim, **2006**.
[22] a) M. Antonietti, *Philos. Trans. R. Soc. London Ser. A* **2006**, *364*, 2817 – 2840; b) S. E. Friberg, C. C. Yang, R. Goubran, R. E. Partch, *Langmuir* **1991**, *7*, 1103 – 1106.
[23] H. K. Bisoyi, S. Kumar, *Chem. Soc. Rev.* **2011**, *40*, 306 – 319.
[24] G. N. Karanikolos, P. Alexandridis, R. Mallory, A. Petrou, T. J. Mountziaris, *Nanotechnology* **2005**, *16*, 2372 – 2380.
[25] A. C. Neville, *Biology of Fibrous Composites*: *Development Beyound the Cell Membrane*, Cambridge University Press, New York, **1993**.
[26] Y. Bouligand, *Tissue Cell* **1972**, *4*, 189 – 217.
[27] Y. Bouligand, V. Norris, *Biochimie* **2001**, *83*, 187 – 192.
[28] a) P. Fratzl, *Collagen*: *Structure and Mechanics*, Springer, New York, **2010**; b) D. Eglin, G. Mosser, M.-M. Giraud-Guille, J. Livage, T. Coradin, *Soft Matter* **2005**, *1*, 129 – 131.
[29] D. Klemm, B. Heublein, H.-P. Fink, A. Bohn, *Angew. Chem. Int. Ed.* **2005**, *44*, 3358 – 3393; *Angew. Chem.* **2005**, *117*, 3422 – 3458.
[30] E. Dujardin, M. Blaseby, S. Mann, *J. Mater. Chem.* **2003**, *13*, 696 – 699.
[31] B. Alonso, E. Belamie, *Angew. Chem. Int. Ed.* **2010**, *49*, 8201 – 8204; *Angew. Chem.* **2010**, *122*, 8377 – 8380.
[32] E. Belamie, M. Y. Boltoeva, K. Yang, T. Cacciaguerra, B. Alonso, *J. Mater. Chem.* **2011**, *21*, 16997 – 17006.
[33] A. D. French, N. R. Bertoniere, R. M. Brown, H. Chanzy, D. G. Gray, K. Hattori, W. Glasser, *Kirk-Othmer Encyclopedia of Chemical Technology*, 5 ed. (Ed.: A. Seidel), John Wiley & Sons Inc., New York, **2004**, pp. 360 – 394.
[34] R. J. Moon, A. Martini, J. Nairn, J. Simonsen, J. Youngblood, *Chem. Soc. Rev.* **2011**, *40*, 3941 – 3994.
[35] Y. Habibi, L. A. Lucia, O. J. Rojas, *Chem. Rev.* **2010**, *110*, 3479 – 3500.
[36] D. Klemm, F. Kramer, S. Moritz, T. Lindström, M. Ankerfors, D. Gray, A. Dorris, *Angew. Chem. Int. Ed.* **2011**, *50*, 5438 – 5466; *Angew. Chem.* **2011**, *123*, 5550 – 5580.
[37] a) B. G. Rånby, *Acta Chem. Scand.* **1949**, *3*, 649 – 650; b) B. G. Rånby, E. Ribi, *Experientia* **1950**, *6*, 12 – 14; c) B. G. Rånby, *Discuss. Faraday Soc.* **1951**, *11*, 158 – 164.
[38] B. L. Peng, N. Dhar, H. L. Liu, K. C. Tam, *Can. J. Chem. Eng.* **2011**, *89*, 1191 – 1206.
[39] J. F. Revol, H. Bradford, J. Giasson, R. H. Marchessault, D. G. Gray, *Int. J. Biol. Macromol.* **1992**, *14*, 170 – 172.
[40] R. H. Marchessault, F. F. Morehead, N. M. Walter, *Nature* **1959**, *184*, 632 – 633.
[41] a) J. F. Revol, D. L. Godbout, D. G. Gray, (Pulp and Paper Research Institute of Canada), US05629055, **1997**; b) J.-F. Revol, L. Godbout, D. G. Gray, *J. Pulp Pap. Sci.* **1998**, *24*, 146 – 149.
[42] K. E. Shopsowitz, H. Qi, W. Y. Hamad, M. J. MacLachlan, *Nature* **2010**, *468*, 422 – 425.
[43] W. Y. Hamad, T. Q. Hu, *Can. J. Chem. Eng.* **2010**, *88*, 392 – 402.
[44] G. von Freymann, V. Kitaev, B. V. Lotsch, G. A. Ozin, *Chem. Soc. Rev.* **2013**, *42*, 2528 – 2554.
[45] H. De Vries, *Acta Crystallogr.* **1951**, *4*, 219 – 226.
[46] X. M. Dong, T. Kimura, J.-F. Revol, D. G. Gray, *Langmuir* **1996**, *12*, 2076 – 2082.
[47] C. C. Y. Cheung, M. Giese, J. A. Kelly, W. Y. Hamad, M. J. MacLachlan, *ACS Macro Lett.* **2013**, *2*, 1016 – 1020.
[48] X. M. Dong, D. G. Gray, *Langmuir* **1997**, *13*, 2404 – 2409.
[49] S. Beck, J. Bouchard, G. Chauve, R. Berry, *Cellulose* **2013**, *20*, 1401 – 1411.
[50] J. Pan, W. Hamad, S. K. Straus, *Macromolecules* **2010**, *43*, 3851 – 3858.
[51] T.-D. Nguyen, W. Y. Hamad, M. J. MacLachlan, *Chem. Commun.* **2013**, *49*, 11296 – 11298.
[52] Y. P. Zhang, V. P. Chodavarapu, A. G. Kirk, M. P. Andrews, *Sens. Actuators B* **2013**, *176*, 692 – 697.
[53] a) E. Belamie, P. Davidson, M. M. Giraud-Guille, *J. Phys. Chem. B* **2004**, *108*, 14991 – 15000; b) J. F. Revol, R. H. Marchessault, *Int. J. Biol. Macromol.* **1993**, *15*, 329 – 335.
[54] a) Q. Liao, Q. Shao, H. Wang, G. Qiu, X. Lu, *Carbohydr. Polym.* **2012**, *87*, 2648 – 2654; b) G. S. Rekhi, S. S. Jambhekar, *Drug Dev. Ind. Pharm.* **1995**, *21*, 61 – 77; c) J. P. F. Lagerwall, C. Schutz, M. Salajkova, J. Noh, J. H. Park, G. Scalia, L. Bergstrom, *NPG Asia Mater.* **2014**, *6*, e80.
[55] a) L. Yan, Q. Zhu, T. Ikeda, *J. Appl. Polym. Sci.* **2001**, *82*, 2770 – 2774; b) R. S. Werbowyj, D. G. Gray, *Macromolecules* **1980**, *13*, 69 – 73.
[56] F.-X. Xiao, J. Miao, B. Liu, *J. Am. Chem. Soc.* **2014**, *136*, 1559 – 1569.
[57] S. Y. Choi, M. Mamak, G. von Freymann, N. Chopra, G. A. Ozin, *Nano Lett.* **2006**, *6*, 2456 – 2461.
[58] H. K. Lee, Y. H. Lee, Q. Zhang, I. Y. Phang, J. M. R. Tan, Y. Cui, X. Y. Ling, *ACS Appl. Mater. Interfaces* **2013**, *5*, 11409 – 11418.
[59] a) K. Ariga, T. Nakanishi, J. P. Hill, *Curr. Opin. Colloid Interface Sci.* **2007**, *12*, 106 – 120; b) K. Sakakibara, J. P. Hill, K. Ariga, *Small* **2011**, *7*, 1288 – 1308.
[60] M. Roman, D. G. Gray, *Langmuir* **2005**, *21*, 5555 – 5561.
[61] D. A. J. Rouquerol, C. W. Fairbridge, D. H. Everett, J. M. Haynes, N. Pernicone, J. D. F. Ramsay, K. S. W. Sing, K. K. Unger, *Pure Appl. Chem.* **1994**, *66*, 1739 – 1758.
[62] S. Lowell, J. E. Shields, M. A. Thomas, M. Thommes, *Characterization of Porous Solids and Powders*: *Surface Area*, *Pore Size and Density*, Kluwer Academic Publisher, Dordrecht, **2004**.
[63] T. Ohsuna, Z. Liu, S. Che, O. Terasaki, *Small* **2005**, *1*, 233 – 237.

[64] M. Giese, M. K. Khan, W. Y. Hamad, M. J. MacLachlan, *ACS Macro Lett.* **2013**, *2*, 818 – 821.
[65] J. A. Kelly, A. M. Shukaliak, C. C. Y. Cheung, K. E. Shopsowitz, W. Y. Hamad, M. J. MacLachlan, *Angew. Chem. Int. Ed.* **2013**, *52*, 8912 – 8916; *Angew. Chem.* **2013**, *125*, 9080 – 9084.
[66] K. Ufuk, M. Min, R. Maren, J. Thomas, W. Gerhard, R. E. Alan, *Model Cellulosic Surfaces*, ACS Symposium Series, *Vol. 1019* (Ed.: M. Roman), American Chemical Society, Washington, DC, **2009**, pp. 137 – 155.
[67] C. T. Kresge, M. E. Leonowicz, W. J. Roth, J. C. Vartuli, J. S. Beck, *Nature* **1992**, *359*, 710 – 712.
[68] a) F. Schüth, *Chem. Mater.* **2001**, *13*, 3184 – 3195; b) P. V. Braun, P. Osenar, S. I. Stupp, *Nature* **1996**, *380*, 325 – 328; c) G. S. Attard, P. N. Bartlett, N. R. B. Coleman, J. M. Elliott, J. R. Owen, J. H. Wang, *Science* **1997**, *278*, 838 – 840; d) K. A. Asghar, J. M. Elliott, A. M. Squires, *J. Mater. Chem.* **2012**, *22*, 13311 – 13317; e) Y. Meng, D. Gu, F. Zhang, Y. Shi, H. Yang, Z. Li, C. Yu, B. Tu, D. Zhao, *Angew. Chem. Int. Ed.* **2005**, *44*, 7053 – 7059; *Angew. Chem.* **2005**, *117*, 7215 – 7221; f) Y. Meng, D. Gu, F. Zhang, Y. Shi, L. Cheng, D. Feng, Z. Wu, Z. Chen, Y. Wan, A. Stein, D. Zhao, *Chem. Mater.* **2006**, *18*, 4447 – 4464; g) D. Feng, Y. Lv, Z. Wu, Y. Dou, L. Han, Z. Sun, Y. Xia, G. Zheng, D. Zhao, *J. Am. Chem. Soc.* **2011**, *133*, 15148 – 15156.
[69] A. Thomas, M. Antonietti, *Adv. Funct. Mater.* **2003**, *13*, 763 – 766.
[70] W. Wang, R. Liu, W. Liu, J. Tan, W. Liu, H. Kang, Y. Huang, *J. Mater. Sci.* **2010**, *45*, 5567 – 5573.
[71] H. Qi, X. Roy, K. E. Shopsowitz, J. K. H. Hui, M. J. MacLachlan, *Angew. Chem. Int. Ed.* **2010**, *49*, 9740 – 9743; *Angew. Chem.* **2010**, *122*, 9934 – 9937.
[72] T.-D. Nguyen, K. E. Shopsowitz, M. J. MacLachlan, *Chem. Eur. J.* **2013**, *19*, 15148 – 15154.
[73] Y. Shin, G. J. Exarhos, *Mater. Lett.* **2007**, *61*, 2594 – 2597.
[74] J. A. Kelly, M. Yu, W. Y. Hamad, M. J. MacLachlan, *Adv. Opt. Mater.* **2013**, *1*, 295 – 299.
[75] K. E. Shopsowitz, J. A. Kelly, W. Y. Hamad, M. J. MacLachlan, *Adv. Funct. Mater.* **2014**, *24*, 327 – 338.
[76] M. A. Brook, Y. Chen, K. Guo, Z. Zhang, J. D. Brennan, *J. Mater. Chem.* **2004**, *14*, 1469 – 1479.
[77] K. E. Shopsowitz, W. Y. Hamad, M. J. MacLachlan, *J. Am. Chem. Soc.* **2012**, *134*, 867 – 870.
[78] A. S. Terpstra, K. E. Shopsowitz, C. F. Gregory, A. P. Manning, C. A. Michal, W. Y. Hamad, J. Yang, M. J. MacLachlan, *Chem. Commun.* **2013**, *49*, 1645 – 1647.
[79] M. Giese, J. C. De Witt, K. E. Shopsowitz, A. P. Manning, R. Y. Dong, C. A. Michal, W. Y. Hamad, M. J. MacLachlan, *ACS Appl. Mater. Interfaces* **2013**, *5*, 6854 – 6859.
[80] K. E. Shopsowitz, W. Y. Hamad, M. J. MacLachlan, *Angew. Chem. Int. Ed.* **2011**, *50*, 10991 – 10995; *Angew. Chem.* **2011**, *123*, 11183 – 11187.
[81] J. A. Kelly, M. Giese, K. E. Shopsowitz, W. Y. Hamad, M. J. MacLachlan, *Acc. Chem. Res.* **2014**, *47*, 1088 – 1096.
[82] G. Siqueira, J. Bras, A. Dufresne, *Polymer* **2010**, *2*, 728 – 765.
[83] V. Favier, H. Chanzy, J. Y. Cavaille, *Macromolecules* **1995**, *28*, 6365 – 6367.
[84] A. Dufresne, *Int. Polym. Process.* **2012**, *27*, 557 – 564.
[85] a) J. M. G. Cowie, G. I. Rodden, *Polymer* **2002**, *43*, 3415 – 3419; b) H. Song, Y. Niu, Z. Wang, J. Zhang, *Biomacromolecules* **2011**, *12*, 1087 – 1096.
[86] A. Cosutchi, C. Hulubei, I. Stoica, S. Ioan, *J. Polym. Res.* **2011**, *18*, 2389 – 2402.
[87] S. N. Fernandes, Y. Geng, S. Vignolini, B. J. Glover, A. C. Trindade, J. P. Canejo, P. L. Almeida, P. Brogueira, M. H. Godinho, *Macromol. Chem. Phys.* **2013**, *214*, 25 – 32.
[88] F. RenChun, D. Jun, H. Hui, G. Zhong-Cheng, *High Perform. Polym.* **2014**, *26*, 27 – 33.
[89] M. Tatsumi, Y. Teramoto, Y. Nishio, *Biomacromolecules* **2012**, *13*, 1584 – 1591.
[90] M. Grunert, W. Winter, *J. Polym. Environ.* **2002**, *10*, 27 – 30.
[91] J. Araki, M. Wada, S. Kuga, *Langmuir* **2001**, *17*, 21 – 27.
[92] L. Heux, G. Chauve, C. Bonini, *Langmuir* **2000**, *16*, 8210 – 8212.
[93] a) M. K. Khan, M. Giese, M. Yu, J. A. Kelly, W. Y. Hamad, M. J. MacLachlan, *Angew. Chem. Int. Ed.* **2013**, *52*, 8921 – 8924; *Angew. Chem.* **2013**, *125*, 9089 – 9092; b) M. Giese, L. K. Blusch, M. K. Khan, W. Y. Hamad, M. J. MacLachlan, *Angew. Chem. Int. Ed.* **2014**, *53*, 8880 – 8884; *Angew. Chem.* **2014**, *126*, 9026 – 9030.
[94] K. E. Shopsowitz, A. Stahl, W. Y. Hamad, M. J. MacLachlan, *Angew. Chem. Int. Ed.* **2012**, *51*, 6886 – 6890; *Angew. Chem.* **2012**, *124*, 6992 – 6996.
[95] S. Kinoshita, *Structural Colors in the Realm of Nature*, World Scientific Publishing Co., Hackensack, **2008**.
[96] a) J. Xu, Z. Guo, *J. Colloid Interface Sci.* **2013**, *406*, 1 – 17; b) K. Yu, T. Fan, S. Lou, D. Zhang, *Prog. Mater. Sci.* **2013**, *58*, 825 – 873.
[97] J. A. Kelly, C. P. K. Manchee, S. Cheng, J. M. Ahn, K. E. Shopsowitz, W. Y. Hamad, M. J. MacLachlan, *J. Mater. Chem. C* **2014**, *2*, 5093 – 5097.
[98] K. Robbie, D. J. Broer, M. J. Brett, *Nature* **1999**, *399*, 764 – 766.
[99] a) R. C. Schroden, M. Al-Daous, C. F. Blanford, A. Stein, *Chem. Mater.* **2002**, *14*, 3305 – 3315; b) G. I. N. Waterhouse, M. R. Waterland, *Polyhedron* **2007**, *26*, 356 – 368; c) C. I. Aguirre, E. Reguera, A. Stein, *Adv. Funct. Mater.* **2010**, *20*, 2565 – 2578; d) S. O. Klimonsky, V. A. Vera, S. S. Alexander, D. T. Yuri, *Russ. Chem. Rev.* **2011**, *80*, 1191.
[100] a) H.-S. Kitzerow, A. Lorenz, H. Matthias (Eds.: H.-S. Kitzerow, A. Lorenz), Wiley-VCH, Weinheim, **2008**; b) H. S. Kitzerow, A. Lorenz, H. Matthias, *Phys. Status Solidi A* **2007**, *204*, 3754 – 3767.
[101] a) J. Ge, Y. Yin, *Angew. Chem. Int. Ed.* **2011**, *50*, 1492 – 1522; *Angew. Chem.* **2011**, *123*, 1530 – 1561; b) Z. L. Wu, J. P. Gong, *NPG Asia Mater* **2011**, *3*, 57 – 64; c) S. A. Asher, J. Holtz, J. Weissman, G. S. Pan, *MRS Bull.* **1998**, *23*, 44 – 50.
[102] D. J. Broer, C. M. W. Bastiaansen, M. G. Debije, A. P. H. J. Schenning, *Angew. Chem. Int. Ed.* **2012**, *51*, 7102 – 7109; *Angew. Chem.* **2012**, *124*, 7210 – 7218.
[103] M. K. Khan, W. Y. Hamad, M. J. MacLachlan, *Adv. Mater.* **2014**, *26*, 2323 – 2328.
[104] W.-E. Lee, Y.-J. Jin, L.-S. Park, G. Kwak, *Adv. Mater.* **2012**, *24*, 5604 – 5609.
[105] Y. Geng, P. L. Almeida, S. N. Fernandes, C. Cheng, P. Palffy-Muhoray, M. H. Godinho, *Sci. Rep.* **2013**, *3*, 1028.
[106] M. R. Islam, X. Li, K. Smyth, M. J. Serpe, *Angew. Chem. Int. Ed.* **2013**, *52*, 10330 – 10333; *Angew. Chem.* **2013**, *125*, 10520 – 10523.
[107] a) R. A. Caruso in *Colloid Chemistry I*, Topics in Current Chemistry *Vol. 226* (Ed.: M. Antonietti), Springer, Berlin, **2003**, pp. 91 – 118; b) H. Liu, G. Wang, J. Liu, S. Qiao, H. Ahn, *J. Mater. Chem.* **2011**, *21*, 3046 – 3052; c) W.-C. Li, G.-Z. Nong, A.-H. Lu, H.-Q. Hu, *J. Porous Mater.* **2011**, *18*, 23 – 30; d) G. S. Armatas, A. P. Katsoulidis, D. E. Petrakis, P. J. Pomonis, M. G. Kanatzidis, *Chem. Mater.* **2010**, *22*, 5739 – 5746; e) T. Waitz, B. Becker, T. Wagner, T. Sauerwald, C. D. Kohl, M. Tiemann, *Sens. Actuators B* **2010**, *150*, 788 – 793.
[108] a) Y. Li, J. Shi, *Adv. Mater.* **2014**, *26*, 3176 – 3205; b) D. Gu, F. Scüth, *Chem. Soc. Rev.* **2014**, *43*, 313 – 344.
[109] a) C. Liang, Z. Li, S. Dai, *Angew. Chem. Int. Ed.* **2008**, *47*, 3696 – 3717; *Angew. Chem.* **2008**, *120*, 3754 – 3776; b) W. Yue, X. Xu, J. T. S. Irvine, P. S. Attidekou, C. Liu, H. He, D. Zhao, W. Zhou, *Chem. Mater.* **2009**, *21*, 2540 – 2546.
[110] a) J. Lee, S. Yoon, T. Hyeon, S. M. Oh, K. B. Kim, *Chem. Commun.* **1999**, 2177 – 2178; b) R. Ryoo, S. H. Joo, S. Jun, *J. Phys. Chem. B* **1999**, *103*, 7743 – 7746; c) M. Tiemann, *Chem.*

Mater. **2008**, *20*, 961 – 971; d) A. H. Lu, F. Schüth, *Adv. Mater.* **2006**, *18*, 1793 – 1805.

[111] a) P. Simon, Y. Gogotsi, *Nat. Mater.* **2008**, *7*, 845 – 854; b) Y. S. Hu, P. Adelhelm, B. M. Smarsly, S. Hore, M. Antonietti, J. Maier, *Adv. Funct. Mater.* **2007**, *17*, 1873 – 1878; c) S. H. Joo, S. J. Choi, I. Oh, J. Kwak, Z. Liu, O. Terasaki, R. Ryoo, *Nature* **2001**, *412*, 169 – 172; d) L. Liao, M. Zheng, Z. Zhang, B. Yan, X. Chang, G. Ji, Z. Shen, T. Wu, J. Cao, J. Zhang, H. Gong, J. Cao, T. Yu, *Carbon* **2009**, *47*, 1841 – 1845.

[112] a) A. B. Fuertes, F. Pico, J. M. Rojo, *J. Power Sources* **2004**, *133*, 329 – 336; b) A. B. Fuertes, G. Lota, T. A. Centeno, E. Frackowiak, *Electrochim. Acta* **2005**, *50*, 2799 – 2805.

[113] A. Ivanova, D. Fattakhova-Rohlfing, B. E. Kayaalp, J. Rathouský, T. Bein, *J. Am. Chem. Soc.* **2014**, *136*, 5930 – 5937.

[114] G. Chu, J. Feng, Y. Wang, X. Zhang, Y. Xu, H. Zhang, *Dalton Trans.* **2014**, *43*, 15321 – 15327.

[115] I. S. Nikolaev, P. Lodahl, W. L. Vos, *J. Phys. Chem. C* **2008**, *112*, 7250 – 7254.

[116] a) H. Qi, K. E. Shopsowitz, W. Y. Hamad, M. J. MacLachlan, *J. Am. Chem. Soc.* **2011**, *133*, 3728 – 3731; b) J. A. Kelly, K. E. Shopsowitz, J. M. Ahn, W. Y. Hamad, M. J. MacLachlan, *Langmuir* **2012**, *28*, 17256 – 17262.

[117] M.-C. Daniel, D. Astruc, *Chem. Rev.* **2004**, *104*, 293 – 346.

[118] a) C. Noguez, I. L. Garzon, *Chem. Soc. Rev.* **2009**, *38*, 757 – 771; b) C. Gautier, T. Bürgi, *ChemPhysChem* **2009**, *10*, 483 – 492; c) V. Kitaev, *J. Mater. Chem.* **2008**, *18*, 4745 – 4749.

[119] a) K. Saha, S. S. Agasti, C. Kim, X. Li, V. M. Rotello, *Chem. Rev.* **2012**, *112*, 2739 – 2779; b) Z. Li, Z. Zhu, W. Liu, Y. Zhou, B. Han, Y. Gao, Z. Tang, *J. Am. Chem. Soc.* **2012**, *134*, 3322 – 3325.

[120] A. P. Alivisatos, *Science* **1996**, *271*, 933 – 937.

[121] a) K. Aoki, D. Guimard, M. Nishioka, M. Nomura, S. Iwamoto, Y. Arakawa, *Nat. Photonics* **2008**, *2*, 688 – 692; b) A. C. Arsenault, T. J. Clark, G. von Freymann, L. Cademartiri, R. Sapienza, J. Bertolotti, E. Vekris, S. Wong, V. Kitaev, I. Manners, R. Z. Wang, S. John, D. Wiersma, G. A. Ozin, *Nat. Mater.* **2006**, *5*, 179 – 184; c) O. Painter, R. K. Lee, A. Scherer, A. Yariv, J. D. O'Brien, P. D. Dapkus, I. Kim, *Science* **1999**, *284*, 1819 – 1821; d) S. Ogawa, M. Imada, S. Yoshimoto, M. Okano, S. Noda, *Science* **2004**, *305*, 227 – 229.

[122] T.-D. Nguyen, W. Y. Hamad, M. J. MacLachlan, *Adv. Funct. Mater.* **2014**, *24*, 777 – 783.

[123] a) P. P. Jha, P. Guyot-Sionnest, *ACS Nano* **2009**, *3*, 1011 – 1015; b) S. S. L. Sobhana, M. V. Devi, T. P. Sastry, A. Mandal, *J. Nanopart. Res.* **2011**, *13*, 1747 – 1757.

[124] a) E. R. Goldman, I. L. Medintz, J. L. Whitley, A. Hayhurst, A. R. Clapp, H. T. Uyeda, J. R. Deschamps, M. E. Lassman, H. Mattoussi, *J. Am. Chem. Soc.* **2005**, *127*, 6744 – 6751; b) J.-S. Yang, T. M. Swager, *J. Am. Chem. Soc.* **1998**, *120*, 5321 – 5322; c) R. Tu, B. Liu, Z. Wang, D. Gao, F. Wang, Q. Fang, Z. Zhang, *Anal. Chem.* **2008**, *80*, 3458 – 3465; d) K. Zhang, H. Zhou, Q. Mei, S. Wang, G. Guan, R. Liu, J. Zhang, Z. Zhang, *J. Am. Chem. Soc.* **2011**, *133*, 8424 – 8427; e) Y. Ma, H. Li, S. Peng, L. Wang, *Anal. Chem.* **2012**, *84*, 8415 – 8421.

[125] a) A. Rose, Z. Zhu, C. F. Madigan, T. M. Swager, V. Bulovic, *Nature* **2005**, *434*, 876 – 879; b) Y. Xia, L. Song, C. Zhu, *Anal. Chem.* **2011**, *83*, 1401 – 1407; c) R. Freeman, T. Finder, L. Bahshi, R. Gill, I. Willner, *Adv. Mater.* **2012**, *24*, 6416 – 6421; d) W. Wei, X. Huang, K. Chen, Y. Tao, X. Tang, *RSC Adv.* **2012**, *2*, 3765 – 3771; e) T. Pazhanivel, D. Nataraj, V. P. Devarajan, V. Mageshwari, K. Senthil, D. Soundararajan, *Anal. Methods* **2013**, *5*, 910 – 916; f) S. S. Nagarkar, B. Joarder, A. K. Chaudhari, S. Mukherjee, S. K. Ghosh, *Angew. Chem. Int. Ed.* **2013**, *52*, 2881 – 2885; *Angew. Chem.* **2013**, *125*, 2953 – 2957.

[126] S. H. M. Mehr, M. Giese, H. Qi, K. E. Shopsowitz, W. Y. Hamad, M. J. MacLachlan, *Langmuir* **2013**, *29*, 12579 – 12584.

[127] a) P. K. H. Ho, D. S. Thomas, R. H. Friend, N. Tessler, *Science* **1999**, *285*, 233 – 236; b) G. Yu, A. J. Heeger, *Synth. Met.* **1997**, *85*, 1183 – 1186; c) A. Teichler, R. Eckardt, C. Friebe, J. Perelaer, U. S. Schubert, *Thin Solid Films* **2011**, *519*, 3695 – 3702; d) A. J. Heeger, *Angew. Chem. Int. Ed.* **2001**, *40*, 2591 – 2611; *Angew. Chem.* **2001**, *113*, 2660 – 2682.

[128] a) D. P. Puzzo, F. Scotognella, M. Zavelani-Rossi, M. Sebastian, A. J. Lough, I. Manners, G. Lanzani, R. Tubino, G. A. Ozin, *Nano Lett.* **2009**, *9*, 4273 – 4278; b) A. Furmanchuk, J. Leszczynski, S. Tretiak, S. V. Kilina, *J. Phys. Chem. C* **2012**, *116*, 6831 – 6840.

[129] L. Feng, H. Li, Y. Qu, C. Lu, *Chem. Commun.* **2012**, *48*, 4633 – 4635.

[130] a) R. C. Smith, W. M. Fischer, D. L. Gin, *J. Am. Chem. Soc.* **1997**, *119*, 4092 – 4093; b) H. Skaff, K. Sill, T. Emrick, *J. Am. Chem. Soc.* **2004**, *126*, 11322 – 11325; c) M. Kyotani, S. Matsushita, M. Goh, T. Nagai, Y. Matsui, K. Akagi, *Nanoscale* **2010**, *2*, 509 – 514.

[131] S. Matsushita, K. Akagi, *Isr. J. Chem.* **2011**, *51*, 1075 – 1095.